



Sedimentary Architecture of Storm-Influenced Tidal Flat Deposits of the Upper Mulichinco Formation, Neuquén Basin, Argentina

Arve R. N. Sleveland^{1*}, Ivar Midtkandal¹, Olivier Galland² and Héctor A. Leanza³

¹ Tectonostratigraphic Research Group, Department of Geosciences, University of Oslo, Oslo, Norway, ² NJORD-Centre, Faculty of Mathematics and Natural Sciences, University of Oslo, Oslo, Norway, ³ Museo Argentino de Ciencias Naturales Bernardino Rivadavia, Buenos Aires, Argentina

OPEN ACCESS

Edited by:

David Mark Hodgson,
University of Leeds, United Kingdom

Reviewed by:

Shahin Dashtgard,
Simon Fraser University, Canada
Cornel Olariu,
The University of Texas at Austin,
United States
Valentina Rossi,
National Research Council (Cnr), Italy

*Correspondence:

Arve R. N. Sleveland
arve.sleveland@gmail.com

Specialty section:

This article was submitted to
Sedimentology, Stratigraphy and
Diagenesis,
a section of the journal
Frontiers in Earth Science

Received: 06 December 2019

Accepted: 25 May 2020

Published: 14 July 2020

Citation:

Sleveland ARN, Midtkandal I,
Galland O and Leanza HA (2020)
Sedimentary Architecture of
Storm-Influenced Tidal Flat Deposits
of the Upper Mulichinco Formation,
Neuquén Basin, Argentina.
Front. Earth Sci. 8:219.
doi: 10.3389/feart.2020.00219

This study reports on the Lower Cretaceous upper Mulichinco Formation in the Neuquén Basin, west-central Argentina. The studied succession comprises shallow marine strata, deposited in a mixed wave and tidal flat environment where ebb-tidal currents dominated. We describe mixed storm- and tide-influenced deposits within progradationally stacked high-frequency sequences and discuss process interaction, sediment dispersal, and preservation potential. These storm and tidal deposits mix spatially on bed, bedset, and sequence scales, suggesting multi-scale process interactions. The study investigates a 12-km-long continuous outcrop, oriented sub-parallel to the paleocoastline. The succession comprises subtidal flat and meandering tidal channel complexes, with interbedding and interfingering of storm and tidal deposits. The tidal deposits are widespread and comprise moderately sorted sandstones with bimodal paleocurrent directions, single and double mud drapes, reactivation surfaces, and inclined heterolithic stratification. Varying bimodal paleocurrent directions suggest that the paleocoastline was irregular, consisting of both protrusions and bays. Storm deposits are mainly found erosively interbedded with subtidal flat sandstones, and exhibit decimeter-thick, well-sorted hummocky and swaley cross-stratified sandstones. These storm deposits show systematic lateral variations in abundance, from dominant to absent, which are linked to subtle variations in water depth along the irregular paleocoastline. As the tidal deposits are widespread across the study area, and with no significant facies change, the varying dispersal of storm-influenced deposits is considered a product of wave refraction, with converging and diverging wave energy at interpreted positions of coastal protrusions and embayments, respectively. Consequently, the irregular paleocoastline morphology caused spatial variability in wave impact and controlled preservation of interbedded storm and tidal deposits at the coastal protrusions while facilitating complete tidal remobilization of sediments in the embayments. With no evidence for fluvial influence, ebb-tidal currents are considered as the main drivers for sediment dispersal onto the subtidal flat, through the meandering tidal channels.

Keywords: mixed-process, tidal, wave, shallow marine, preservation, Mulichinco Formation, Neuquén Basin

INTRODUCTION

Shallow marine and coastal deposits are commonly classified with respect to their dominant depositional and modification processes (fluvial, wave, and tidal) on ternary diagrams (e.g., Galloway, 1975; Boyd et al., 1992; Dalrymple et al., 1992; Ainsworth et al., 2011). The classification schemes are typically used to infer certain depositional styles and three-dimensional (3D) architecture, based on the interpreted depositional environment, and have implications for predictive models for sediment body distribution. Ternary diagrams therefore offer a means of guiding our expectation of sediment distribution within a depositional system, but predictions of heterogeneity in depositional process distribution both within that system and along the paleo-strike are limited. Furthermore, ternary diagrams do not account for how paleogeography and paleotopography/bathymetry impact process distribution within a sedimentary environment, ultimately affecting the 3D architecture of a deposit. Shallow marine and coastal systems are highly dynamic environments where relative dominance of depositional processes, their relative contribution, distribution, and level of interaction may shift through time and space (Ainsworth et al., 2011; Vakarelov and Ainsworth, 2013; Olariu, 2014; Rossi et al., 2017). For such systems, multiple ternary diagrams can be applied together to better explain and classify the spatiotemporal development and distribution of architectural elements (Ainsworth et al., 2011). Where fluvial influence is low/absent, such as in a tidal flat or shoreface environment, a ternary diagram can be helpful to distinguish between fair-weather and storm waves and their contribution relative to tidal processes (Dashtgard et al., 2012).

Mixed-process coastal deposits can be divided into two main types. First, there are deposits that form in separate domains of process dominance. These are environments where process dominance is restricted by morphology, such as in a barrier island complex (wave dominance), back-barrier tidal lagoons and channels, and potentially a fluvial-dominated bay-head delta landward. Examples of such present-day environments are the Friesian Islands coastline of the Netherlands (shown in Sixsmith et al., 2008, Figure 15) or the barrier-bay systems of the northern Gulf of Mexico (Simms et al., 2006; Rodriguez et al., 2010). Similar ancient examples include the Upper Cretaceous Cliff House Sandstone (Donselaar, 1989; Olsen et al., 1999) and Hosta Tongue Sandstone (Sixsmith et al., 2008) of New Mexico, United States, the Upper Cretaceous Sego Sandstone of Utah and Colorado, United States (e.g., Willis and Gabel, 2001, 2003; Painter et al., 2013; Legler et al., 2014; Burton et al., 2016), and the Middle Jurassic Lajas Formation of the Neuquén Basin, west-central Argentina (e.g., Rossi and Steel, 2016). In such coastal environments, process interaction is limited to the transition zones between the sections of process dominance (Rossi and Steel, 2016, Figures 20, 21), but the domains can shift through time, resulting in a successive mix of deposits in the rock record. Second, there are deposits that form by a dynamic interaction of processes, where relative process contribution is approaching equal. This means that the interaction of coastal processes may vary by seasonal variations in fluvial discharge, the frequency and magnitude of storms or the wave impact, and how these combine

with tidal currents during neap and spring cycles. The successive alternation of storm and tidal deposits in the deltaic Rannoch Fm., Northern North Sea (Wei et al., 2016), is an example of how storm waves and tidal currents have altered the architecture of a delta shoreface by successively remobilizing each other's deposits. Other examples of similar process interactions have been recognized from other depositional systems where waves and tides interacted on deposition (Yang et al., 2005; Dashtgard et al., 2009, 2012; Vakarelov et al., 2012; Leva López et al., 2016; Vaucher et al., 2017) and paleoenvironments that also recorded some degree of fluvial influence (Jordan et al., 2016; Van Cappelle et al., 2017; Peng et al., 2018).

In mixed-process coastal environments, fluvial, wave, and tidal processes all have the capacity to modify and redistribute sediments, which adds complexity and clutters our understanding of initial sediment partitioning, sorting, textures, internal structures, and sediment body distribution. What is preserved from such dynamic coastal environments is not a complete archive of processes active in the basin. To understand the distribution of such mixed-process deposits relies on the accurate unraveling of the intrinsic behavior of their parental processes, and their spatiotemporal interaction.

To constrain the process interplay in an ancient depositional environment, its preservation potential must be considered. It has long been recognized that the preserved stratigraphic record is incomplete and filled with temporal hiatuses, which span from years to millions of years (Sadler, 1981; Miall, 2015; Holbrook and Miall, 2020). For this reason, calculations of sedimentation rates are time scale-dependent and inaccurate (Sadler, 1981), and the stratigraphic record is thus unrepresentative in explaining the true development of a sedimentary environment (Miall, 2015). Because of the high potential for having unpreserved (missing) strata in a sedimentary succession, investigations of true process interplay are challenging. Additionally, preservation of storm- and tide-generated deposits may vary according to grain size, following the different stages of the relative sea level cycle (Yoshida et al., 2007). Yoshida et al. (2007) presented how storm-generated structures are better preserved in fine and very fine sand and associated to transgressive and highstand coastlines, while current-driven (such as tidal) structures are typically favored in medium and coarse sand from falling stage and early lowstand coastlines.

In a setting where the sediment caliber and water depth allow for storms and tidal currents to rework the same sediment, tidal currents are relentless along a (tidally active) coastline (e.g. Dalrymple, 2010; Dean et al., 2019), while storm waves are relatively short-lived surges of higher energy (e.g. Duke, 1985; Collins et al., 2017). This way, at constant tidal energy, storms may exert greater impact on the preserved sediment than tides (Vakarelov et al., 2012), depending on storm frequency and magnitude. Storm frequency controls the number of storm beds within a succession, while storm magnitude controls storm bed thicknesses (Duke, 1985; Clifton, 2006). Low-frequency/magnitude storms, relative to constant tidal energy, favor tidal remobilization of their relatively thin storm deposits, while high-frequency/magnitude storms favor complete wave reworking of tidal deposits. Both end-members can erase the opposing process completely, leaving the rock record empty of

any signs that may help identify a mix of coastal processes. Ancient shallow marine deposits can therefore be classified as end-member single-process depositional environments, even though they could have formed in mixed-process environments (Vakarelov et al., 2012). Adding to this intrinsic complexity, wave energy is not uniformly distributed along all coastlines. Irregular coastlines experience wave refraction, where waves (and thereby wave energy) converge/concentrate around coastal protrusions (or shallowing bathymetry) and diverge in bays (e.g., Swift and Thorne, 1991). Consequently, the relative interplay between waves and tidal currents and their relative contribution and dominance depend on coastline morphology/bathymetry and storm frequency/magnitude.

To further the understanding of sedimentary architecture where wave and tidal processes dynamically interact, a field study has been conducted on the shallow marine Lower Cretaceous (Valanginian) Mulichinco Formation (Fm.) in the Neuquén Basin, west-central Argentina (Howell et al., 2005; Schwarz and Howell, 2005; Schwarz et al., 2006). We identify and describe mixed wave- and tide-influenced deposits within the upper Mulichinco Fm. and discuss sediment partitioning, dispersal, and preservation in this complex marginal marine environment.

GEOLOGIC FRAMEWORK AND STRATIGRAPHY

The Upper Triassic to Lower Cenozoic Neuquén Basin is situated in west-central Argentina, between 32° and 40° South latitude, and covers an area of about 120,000 km² (Figure 1A). This basin comprises a nearly 40,000-m-thick sedimentary succession, deposited in a retro-arc basin embayment that evolved into a foreland basin during the Lower Cretaceous, on the eastern side of the Andean Cordillera (Howell et al., 2005). The Neuquén Basin was bordered by the cratonic Sierra Pintada System to the east and the North Patagonian Massif to the south and has remained open to the north and partially to the west through the proto-Andean volcanic arc (Howell et al., 2005) (Figure 1A). Three main tectonic stages initiated and acted upon the Neuquén Basin deposition: (1) the Upper Triassic-Lower Jurassic syn-rift stage, which initiated the basin formation; (2) the Lower Jurassic-Lower Cretaceous postrift/back-arc, ramp-type basin stage; and (3) the Lower Cretaceous-Cenozoic foreland basin stage (Legarreta and Uliana, 1991; Franzese et al., 2003; Howell et al., 2005). Continued Cenozoic contractional tectonism exhumed parts of the Neuquén Basin stratigraphy, which is folded and deformed in the west, while nearly undeformed in the east (Vergani et al., 1995; Franzese et al., 2003; Schwarz and Howell, 2005).

The Neuquén Basin sedimentary succession reflects deposition in continental, shallow marine, and deep marine environments, through multiple transgressive–regressive (T/R) cycles (Vergani et al., 1995; Howell et al., 2005). In the context of a low-gradient ramp basin, the central Neuquén Basin contains Tithonian to Lower Valanginian organic-rich mudstones of the Vaca Muerta Fm., which was deposited in a tidally dominated carbonate-siliciclastic ramp setting (Spalletti et al., 2000). The Vaca Muerta Fm. is overlain by Valanginian continental, shallow

marine, and inner shelf-mixed carbonate-siliciclastic deposits of the Mulichinco Fm. (Figure 1B) (Legarreta and Gulisano, 1989; Howell et al., 2005; Schwarz et al., 2006). The up to 400-m-thick Mulichinco Fm. is subdivided into three informal members: the lower, middle, and upper members (Figure 1B) (Schwarz, 1999), according to their regressive, transgressive, and regressive development, respectively. For the purpose of simplicity, these informal subunits are hereafter referred to as the lower, middle, and upper Mulichinco Fm.

The lower Mulichinco Fm. represents a progradational succession of fluvial and flood plain deposits in the south, which grade and interfinger northward into beach- and heterolithic shallow marine strata. Bounded by a transgressive surface, the lower Mulichinco Fm. is overlain by a laterally extensive retrogradational succession of carbonate ramp deposits, which belong to the middle Mulichinco Fm. (Schwarz and Howell, 2005). The middle Mulichinco Fm. contains three coarsening- and shallowing-up oyster- and bivalve-rich carbonate parasequences (*sensu* Catuneanu et al., 2009), with ammonite body fossils (Schwarz and Howell, 2005; Schwarz et al., 2006). The upper Mulichinco Fm. comprises a progradational succession that grades from mud-rich bay-fill in the south to sand-rich shallow marine deposits in the north-northwest (Schwarz and Howell, 2005; Schwarz et al., 2006). These shallowing-up units are locally capped by decimeter-thick oyster and shell gravel carbonate beds, formed during low-sediment influx periods of transgression or non-deposition (Schwarz, 2012; Schwarz et al., 2013, 2016). The Upper Valanginian recorded the onset of basin-wide transgression (Vergani et al., 1995), which is reflected through retrogradational stacking of the uppermost Mulichinco Fm. This transgression ultimately flooded the Mulichinco Fm. strata and formed the overlying carbonates and euxinic mudstones of the lowermost Agrio Fm. (Figure 1B) (Vergani et al., 1995).

The Mulichinco Fm. offers several-kilometer-long, high-quality outcrops along the flanks of eroded anticlines of the Chos Malal fold and thrust belt (Figure 1C). This study examines the upper Mulichinco Fm. as expressed in a ca. 12-km-long outcrop in the eastern foothills of the Tromen Volcano (Figures 1B,D), which crops out as steeply dipping layers (50°–60°) and is part of the tight ramp anticline of the Tromen Thrust (Galland et al., 2007). Schwarz and Howell (2005) and data from this study suggest that the outcrop is oriented sub-parallel to the paleocoastline, which makes it an excellent candidate for studies of along-strike variability of sediment dispersal and architecture.

METHODS AND DATASET

The dataset includes (1) four measured sections from Cerro Pampa Tril, Pampa Tril, Barranca Los Loros, and Río Pequenco localities (Figure 1D), where stratigraphic variation and sedimentary composition have been determined through descriptive sedimentology. The measured sections (150–210 m thick) include the exposed upper Mulichinco Fm., and document the stratigraphic succession at 1:100 scale. Paleocurrent reconstructions from the interval of focus in this study were calculated from collected strike/dip measurements,

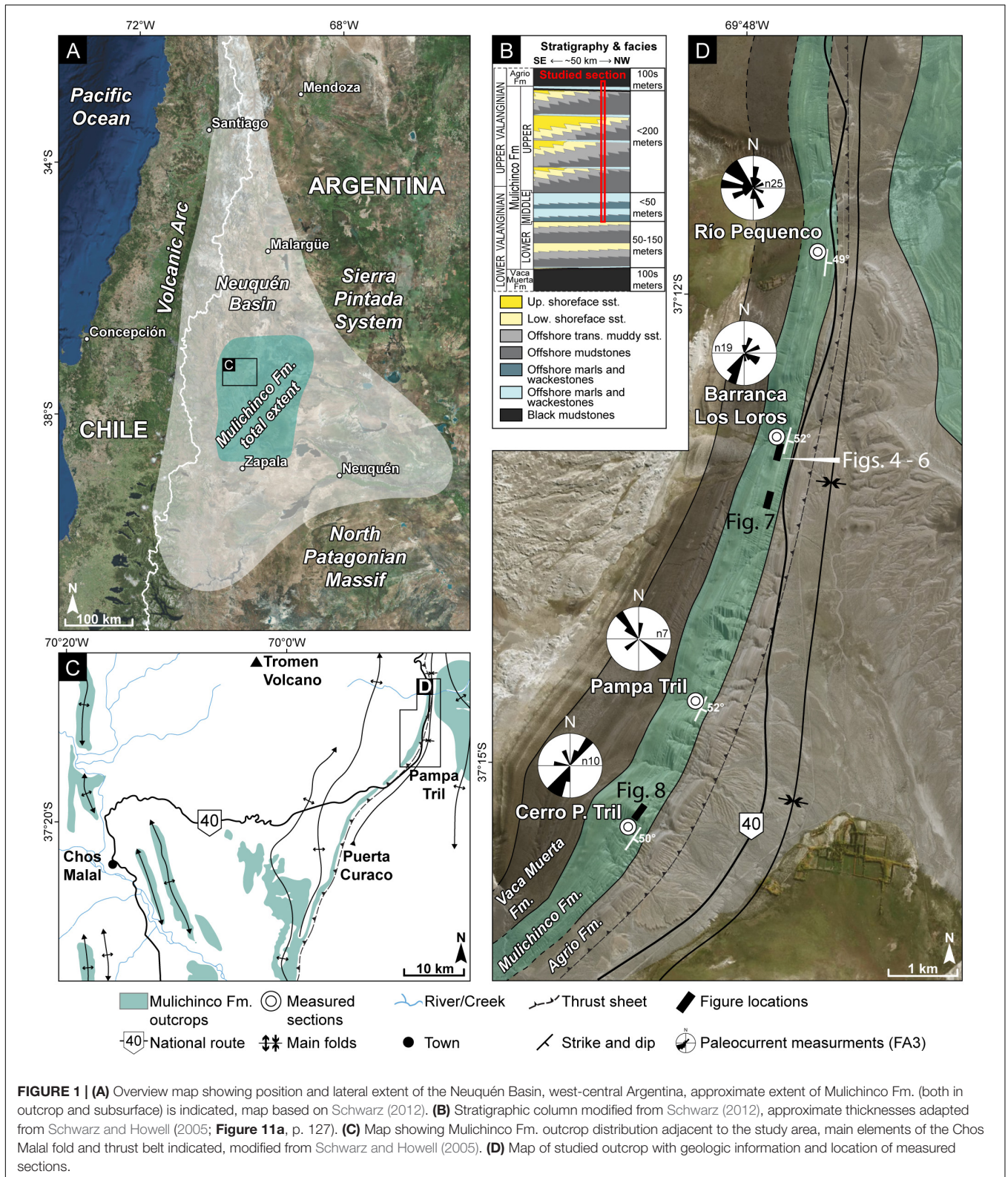


FIGURE 1 | (A) Overview map showing position and lateral extent of the Neuquén Basin, west-central Argentina, approximate extent of Mulichinco Fm. (both in outcrop and subsurface) is indicated, map based on Schwarz (2012). **(B)** Stratigraphic column modified from Schwarz (2012), approximate thicknesses adapted from Schwarz and Howell (2005; Figure 11a, p. 127). **(C)** Map showing Mulichinco Fm. outcrop distribution adjacent to the study area, main elements of the Chos Malal fold and thrust belt indicated, modified from Schwarz and Howell (2005). **(D)** Map of studied outcrop with geologic information and location of measured sections.

which were subsequently back-rotated according to the bedform's structural strike/dip values to obtain true paleocurrent directions. Bioturbation intensity (BI) was recorded following a

0–6 grade indexing scale (Bann et al., 2004), originally adapted from Reineck (1963) and Taylor and Goldring (1993). BI 0 means that bioturbation is absent, and BI 6 means complete

bioturbation and total biogenic homogenization of the sediment (Bann et al., 2004). Carbonate facies were classified according to Wright (1992), who revised classifications from Dunham (1962) and Embry and Klovan (1971). Ternary diagrams from Dashtgard et al. (2012) were populated with visual estimates of process distribution at and between the four localities of this study; they are intended as graphical guides and not absolute measurements of process distribution. (2) Photographs were taken at and between the localities to document sedimentary structures, facies transitions, and bounding relations. (3) Aerial photographs, taken from an unmanned aerial vehicle, were used to construct (4) 3D Virtual Outcrop Models (VOMs), following the structure-from-motion photogrammetry principles of Westoby et al. (2012). VOMs were constructed in Agisoft Metashape Pro v1.5.0 (Agisoft LLC, St. Petersburg, Russia), and 3D interpretation was conducted in LIME (Buckley et al., 2019), a 3D visualization and interpretation software developed by Virtual Outcrop Geology Group at NORCE Norwegian Research Centre, Bergen, Norway. A VOM allows distortion-free orthorectified outcrop images to be generated, improving confidence in sedimentary architecture analysis. Four high-resolution (2-cm resolution) VOMs were generated to help constrain spatial distribution of architectural elements at each locality. One 50-cm resolution VOM that covers the complete 12-km-long outcrop was constructed to establish a stratigraphic surface framework between (and beyond) the four measured sections.

Based on the acquired data, a model is presented (Figure 13) to schematically illustrate how climatic changes in storm frequency and magnitude impacted on the depositional signature of a mixed storm- and tide-influenced sedimentary succession and how the impact of wave refraction has a comparable depositional signature to these climatic parameters. This conceptual model relies on constant subsidence rate and tidal energy. Relative storm frequency and magnitude are read from the x and y axes, respectively. To be valid, the plotted data need to originate from the same depositional environment. Storm bed thicknesses are plotted on the storm magnitude axis, while storm frequency is derived from the number of storm beds within every 5 m of the measured sections. Supplemental and approximate data gathered from the VOMs are plotted as well.

RESULTS: SEDIMENTOLOGY AND DEPOSITIONAL ENVIRONMENTS

We report on the upper Mulichinco Fm. depositional development and architecture, utilizing the established stratigraphic framework from Schwarz and Howell (2005) and Schwarz et al. (2006) in light of the high-frequency sequences described and demonstrated by Schwarz (2012) and Schwarz et al. (2013, 2016). Sedimentary facies (18) are presented in Table 1 and construct the basis for the (6) facies associations (FAs) that are described and discussed in this paper. FAs are presented in ascending stratigraphic order. Selected sedimentary facies are shown in Figure 2.

Facies Associations

FA1—Carbonate Deposits

Description

FA1 comprises tabular and extensive (tens of kilometers) 2- to 10-m-thick carbonate units. FA1 coarsens up from basal mud- and floatstones (Facies A), with scarce crushed skeletal material that increase in size and abundance upward into compact and structureless rudstones (Facies B) (Figure 2A), which are locally capped by 0.1- to 0.5-m-thick tabulate coral framestones (Facies C). Rudstones generally occur in meter-thick tabular beds with densely packed crushed shell gravel and up to decimeter-sized complete and upright bivalves and oysters. Ammonite body fossils (5- to 25-cm diameters) are abundant at the top of oyster rudstones (Figure 2A), most commonly found in the south, at Cerro Pampa Tril and Pampa Tril (Figure 1D). *Thalassinoides* trace fossils occur (BI 1) (Figures 3A,B). FA1 is found throughout the studied succession, as decimeter-thick units covering FA2 deposits, albeit it is most dominant in the lower stratigraphic section where three stacked FA1 units are mapped as the middle Mulichinco Fm.

Interpretation

FA1 represents upward shallowing carbonate cycles that developed during periods of low siliciclastic influx on a low angle ramp profile (Schwarz and Howell, 2005; Schwarz et al., 2013). Mud- and floatstones were deposited from suspended load below fair-weather wave base, as they contain scarce skeletal material. Fair-weather waves provided habitable conditions for oysters and bivalves, which were packed into rudstones from natural biological activity and waves (Lazo, 2007; Schwarz et al., 2016, 2018). Coral framestones developed laterally as isolated patch reefs.

FA2—Offshore to Lower Shoreface

Description

FA2 is mud-dominated and consists of several-meters-thick laminated mudstones (Facies F) (Figure 2B) at the base, which transitions at the top into an interbedded succession with well-sorted, very fine, and fine-grained hummocky cross-stratified (HCS) sandstones (Facies G) (Figures 2D,E). Decimeter-thick beds of disorganized shell gravel with basal low-angle, cross-laminated sandstone clasts (Facies D) (Figure 2C) occur. HCS sandstones occur as upward thickening 5- to 20-cm-thick layers, are laterally extensive (several tens of meters to a few kilometers), and interbedded with equally thick successions of laminated mudstones. Interbedded mudstones and HCS sandstones are arranged in up to 1.5-m-thick bedsets at the top of FA2. Rare *Thalassinoides* trace fossils are recorded in the mudstones (BI 1), and sporadic *Gyrochorte* (Figures 3B–F) and *Ophiomorpha* (Figures 3C,E,G) trace fossils are found in the HCS sandstones (BI 1–4). FA2 grades or sharply transitions upward into FA1, FA2, or FA3 deposits. Where FA2 is overlain by FA2, this is recognized where interbedded HCS sandstones and mudstones of FA2 sharply transitions upward into several meters thick FA2 mudstone deposits. Where FA2 is overlain by FA3, this is marked by a sharp increase in grain-size, from mud-dominated FA2 to sand-dominated FA3.

TABLE 1 | Recorded sedimentary facies in the middle and upper Mulichinco Fm., facies are grouped according to their defining signature, and subordinately arranged in ascending stratigraphic order.

Defining signature	Facies	Description	Structures/composition	Grain size	Trace fossils	Depositional interpretation	Dominant depositional/modification process
Carbonate	A	Carbonate mud	Loosely packed carbonate mudstone to wackestone containing finely crushed (mm scale) shell fragments	Mudstone, Floatstone < 2cm shell fragments		Passive deposition on carbonate ramp	–
	B (Figure 2A)	Oyster gravel bed, rudstone	Densely packed, finely to moderately crushed, cm-scale, oyster-, and bivalve shell fragments. Carbonate mud matrix with occasional complete oysters and bivalves preserved in upright position, commonly toward bed top. Ammonite body fossils occur in southern extent of study area	Rudstone, <10 cm shell fragments	<i>Thalassinoides</i>	Open marine shell bank	Fair-weather waves
	C	Coral framestone	Densely packed framestone constructed by 3–15 cm long branched tabulate corals	Framestone		<i>In situ</i> preservation of coral patch reef	Fair-weather waves
	D (Figure 2C)	Disorganized shell gravel	Crushed shell gravel bed, disorganized arrangement, occasional tabulate coral fragments, sharp bed boundaries, erosive base with occasional ellipsoid-shaped (3 × 10 cm) sandstone rip-up clasts with low-angle cross-lamination	Rudstone-VF		Storm-reworked and -remobilized carbonate material	Storm waves
	E	Cross-stratified oolite grainstone	Densely packed oolite with undifferentiated crushed (>2 cm) shell fragments, meter-scale trough-, tangential-, and sigmoidal cross-stratification, sets <5-m thick	Grainstone, <1 cm shell fragments		Deposition by tractional flow, reworked and transported ooid and skeletal material, organized in dunes	Tidal currents
Well sorted siliciclastics	F (Figure 2B)	Laminated mudstone	Plane parallel-laminated mudstone, gray to green	Mud	<i>Thalassinoides</i>	Deposition from suspension in quiescent water conditions	–
	G (Figures 2D,E)	Hummocky cross-stratified sandstone	Hummocky cross-stratified, homogeneous sandstone. Stratification amplitude 5–40 cm, wavelength 50–210 cm	VF	<i>Gyrochorte</i> , <i>Ophiomorpha</i>	Deposition by storm wave oscillation, between fair-weather and storm wave base, shallow marine ichnofauna	Storm waves
	H (Figure 2F)	Swaley cross-stratified sandstone	Swaley cross-stratified, homogeneous sandstone, convolute bedding occurs, trough dimensions 10–40-cm-thick, 30–120-cm-wide	VF-M	<i>Thalassinoides</i> , <i>Ophiomorpha</i>	Deposition and erosion by storm wave oscillation, convolute bedding reflects rapid waterlain deposition and subsequent collapse by dewatering, shallow marine ichnofauna	Storm waves

(Continued)

TABLE 1 | Continued

Defining signature	Facies	Description	Structures/composition	Grain size	Trace fossils	Depositional interpretation	Dominant depositional/modification process
Moderately sorted siliciclastics	I	Low angle cross-stratified sandstone	Very well sorted, subhorizontal- to low-angle cross-stratified sandstone with occasional mud-draped horizons	VF-F		Upper oscillatory regime (Arnott, 1993) and short-lived periods of standing water conditions to deposit mud-draped horizons	Storm waves
	J (Figure 2G)	Trough cross-stratified sandstone	Trough cross-stratified sandstone, tangential bottomset terminations, occasional mud-chip rip-up clasts, shell gravel along bottomsets occur	VF-F, <3 cm shell fragments		Deposition of 3D dunes, tangential bottomset terminations indicate flow separation at dune crests, clast-bearing lags are due to erosive transport and rapid deposition	Storm waves
	K (Figures 2H–J)	Trough cross-stratified sandstone with reactivation surfaces	Trough cross-stratified sandstone, herringbone cross-stratification common, tangential bottomset terminations, undulating erosive dune bases, internal truncation surfaces, shell gravel along bottomsets common, occasional mud-chip rip-up clasts	VF-F, <3 cm shell fragments	<i>Arenicolites</i>	Deposition of 3D dunes by flowing water, herringbone structures suggest current reversals, tangential bottomset terminations indicate flow separation at dune crests, undulating erosive bases testify sequential flow velocity alterations, where these erosional bases separate foresets that migrate in the same direction, they represent reactivation surfaces	Tidal currents
	L (Figures 2K,L)	Asymmetric and combined flow ripple cross-laminated sandstone	Asymmetric and combined flow ripple cross-laminated sandstone, mud-draped foresets, and -bedding planes abundant	VF-F		Deposition by unidirectionally flowing water in lower flow regime, mud-drapes testify periodic quiescent water conditions, combined flow ripples testify reworking by oppositely directed flow and/or wave oscillation	Tidal currents
	M	Bundled symmetric ripple cross-laminated sandstone	Symmetric ripple cross-laminated sandstone, bundled upbuilding, ripple-bounding mud-drapes occur	VF-F		Deposition in shallow water conditions, wave oscillation is dominant, mud draping during standing water, and swash-movement causes bundling and trouphy internal structure	Fair-weather waves

(Continued)

TABLE 1 | Continued

Defining signature	Facies	Description	Structures/composition	Grain size	Trace fossils	Depositional interpretation	Dominant depositional/modification process
	N	Climbing ripple cross-laminated sandstone	Climbing ripple cross-laminated sandstone, occasionally mud-draped ripple-bounding horizons	VF-F		Rapidly decreasing unidirectional flow velocity causes rapid deposition of suspended load material and preservation of both stoss and lee side of ripple (Allen, 1973; Nichols, 2009, p.53)	Tidal currents
	O (Figure 2M)	Lenticular-bedded heterolith	Oppositely directed asymmetric ripple cross-laminated sandstone lenses in matrix of laminated mudstones	Mud, VF-F	<i>Thalassinoides</i> , <i>Gyrochorte</i>	Fluctuations between flowing and quiescent water conditions, current reversals, shallow marine ichnofauna	Tidal currents
	P (Figure 2N)	Wavy-bedded heterolith	Compound symmetric-, and asymmetric ripple cross-laminated sandstones systematically interbedded with laminated mudstones, mud-drapes and bidirectional paleocurrent directions identified	Mud, VF-F	<i>Thalassinoides</i> , <i>Gyrochorte</i> , <i>Ophiomorpha</i> , <i>Spongeliomorpha</i> , <i>Palaeophycus</i>	Fluctuations between flowing and quiescent water conditions, higher energy than Facies O, current reversals, shallow marine ichnofauna	Tidal currents
	Q (Figure 2O)	Flaser-bedded sandstone	Heterogeneous, mud-draped, asymmetric ripple-laminated sandstone, abundant internal erosional truncation surfaces	Mud, VF-F	<i>Thalassinoides</i> , <i>Ophiomorpha</i>	Fluctuations between flowing and quiescent water conditions, higher energy than Facies P, potentially internal reactivation surfaces, shallow marine ichnofauna	Tidal currents
Mottled	R	Structureless sandstone	Massive/structureless sandstone	VF-F		Rapid deposition by suspension, or turned completely massive by bioturbation, or crystalline cementation may disturb visibility of primary structures	–
	S	Bioturbated sandstone	Mottled-, completely bioturbated sandstone, limited to no original sedimentary structures preserved, various degree of burrow structure preservation, internal erosional bedding surfaces	VF-F		Substantial pause in sediment input and consequent complete bioturbation of deposits, shallow marine ichnofauna	–

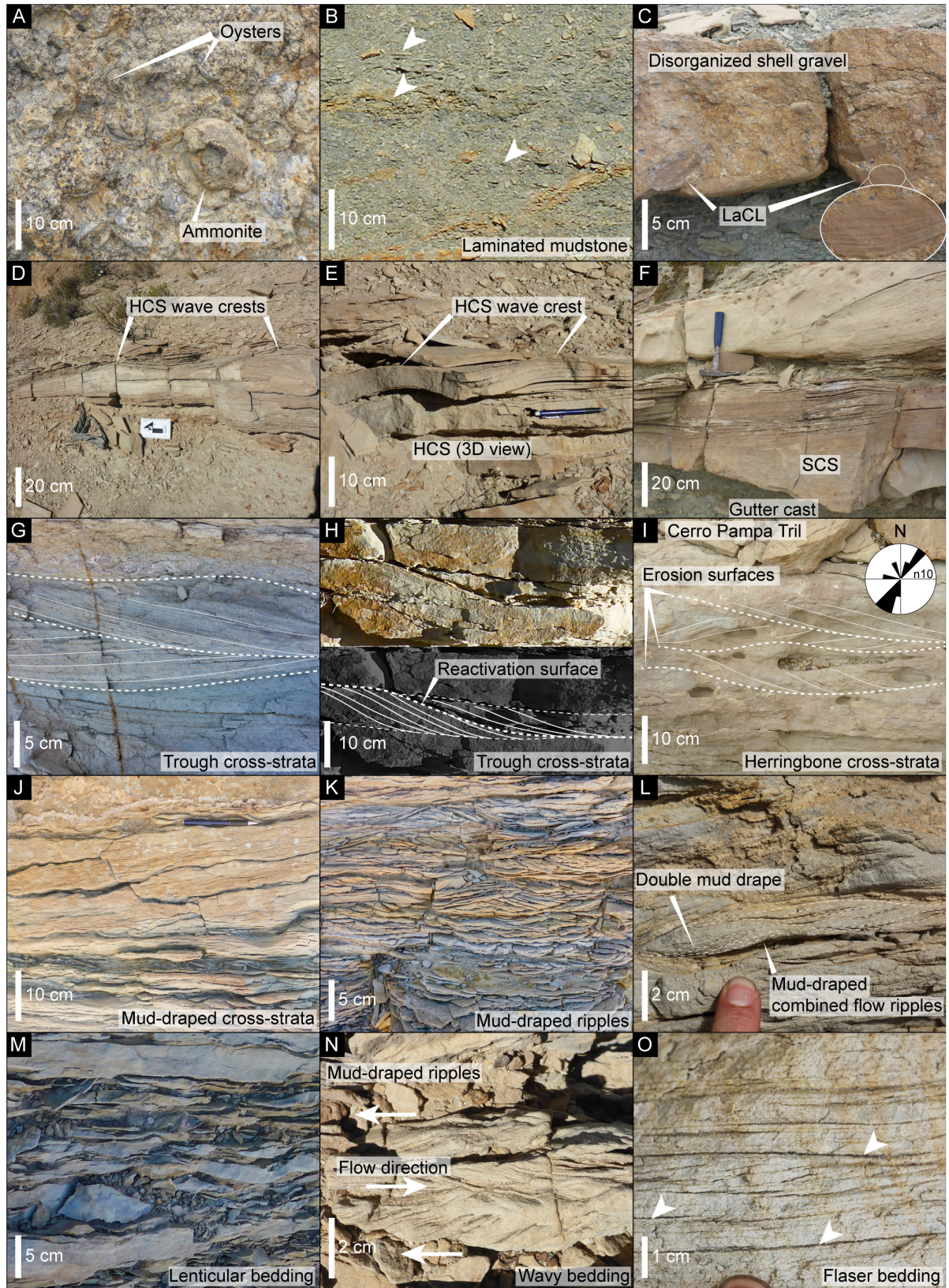


FIGURE 2 | Continued

FIGURE 2 | Overview of selected sedimentary structures recorded in the middle and upper Mulichinco Fm. (cf. **Table 1**). **(A)** Oyster gravel bed with ammonite (Facies B). **(B)** Laminated mudstone (Facies F); white arrows point to lamination. **(C)** Disorganized shell gravel with basal sandstone clasts (Facies D). **(D)** HCS with indicated wave crests (Facies G). **(E)** Overview of HCS (Facies G). **(F)** SCS with gutter cast (Facies H). **(G)** Trough cross-strata (Facies K). **(H)** Trough cross-strata with reactivation surface (Facies K). **(I)** Trough cross-strata with herringbone structures (Facies K); photo and paleocurrent data from Cerro Pampa Tril. **(J)** Mud-draped toesets in trough cross-strata (Facies K). **(K)** Asymmetric and combined flow ripples (Facies L). **(L)** Mud-draped combined flow ripples (Facies L). **(M)** Lenticular bedding (Facies O). **(N)** Herringbone in wavy bedding (Facies P). **(O)** Flaser bedding (Facies Q).

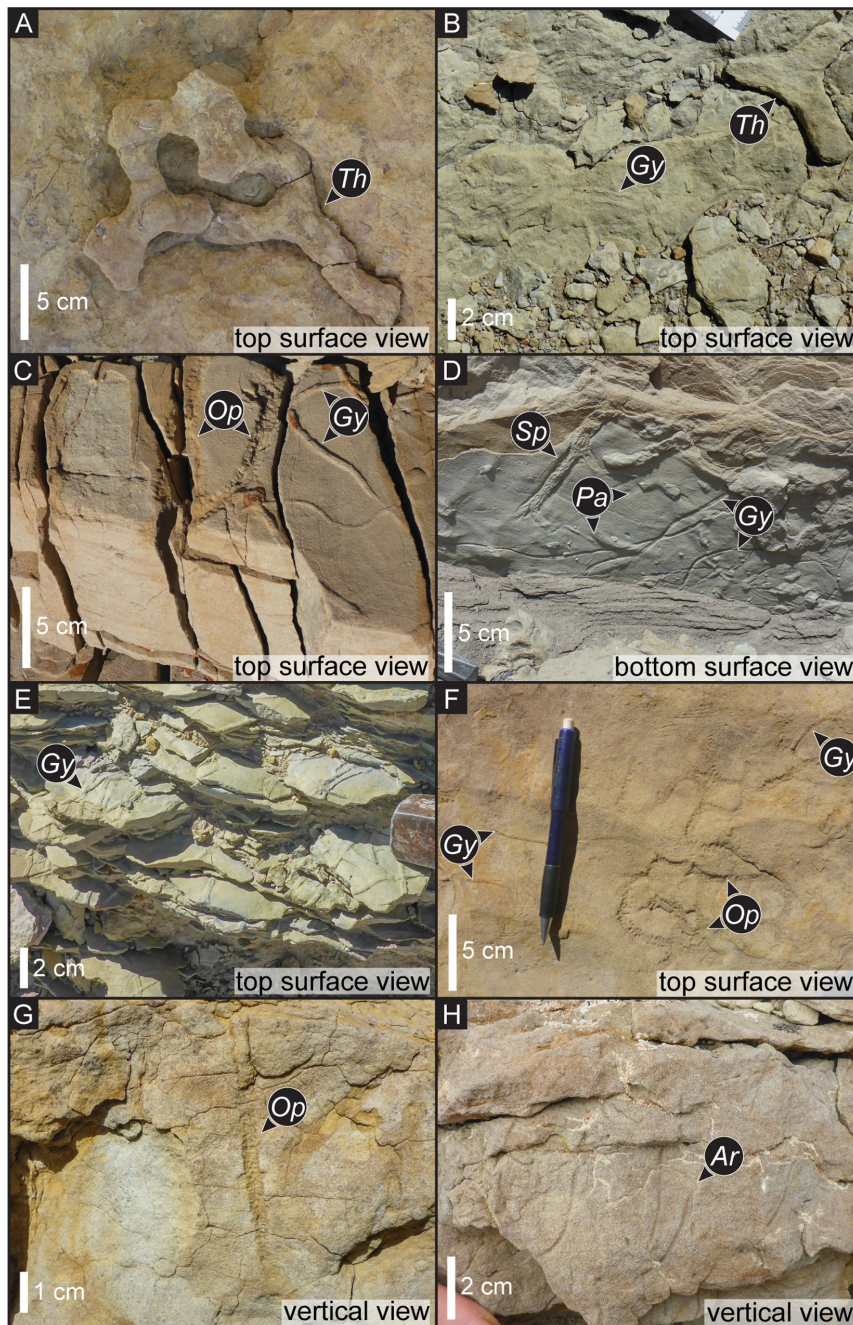


FIGURE 3 | Representative overview of recorded fossils—*Thalassinoides* (Th), *Gyrochorte* (Gy), *Ophiomorpha* (Op), *Spongiomorpha* (Sp), *Palaeophycus* (Pa), and *Arenicolites* (Ar); photographs cover selected facies and are not meant as indicating exclusivity of trace fossil. **(A)** Flaser bedding top surface view (Facies Q). **(B)** Wavy bedding top surface view (Facies P). **(C)** HCS top surface view (Facies G). **(D)** Wavy bedding bottom surface view (Facies P). **(E)** Lenticular bedding top surface view (Facies O). **(F)** Wavy bedding top surface view (Facies P). **(G)** SCS vertical view (Facies H). **(H)** Trough cross-strata with reactivation surfaces vertical view (Facies K).

Interpretation

FA2 reflects upward shallowing units from offshore to lower shoreface environments. The several-meters-thick accumulations of laminated mudstones in lower FA2 suggest a low-energy depositional environment where sedimentation occurred from suspended load material. HCS deposits are typically associated with the lower shoreface and offshore transition (Harms et al., 1975), and it is therefore interpreted that FA2 represents deposits that grade up from offshore (laminated mudstone) into a lower shoreface environment, where storm waves reworked and remobilized sand and deposited HCS sandstones. Disorganized shell gravel reflects storm reworking of shells on the shelf, and the preservation of low-angle, cross-laminated sandstone clasts at their base suggests that the sandstones were at least semi-consolidated or lithified prior to the storm event that formed the disorganized shell gravel. This facies relationship can have two explanations—either that carbonate production in the system provided very early cementation for the sandstone beds or that a substantial hiatal surface is located between the two deposits, allowing for the sandstone beds to semi-consolidate before they were incorporated into Facies D deposits. The presence of a hiatal surface means that bored hardgrounds could be expected to be found in the succession, but we have not observed this facies.

FA3—Storm-Influenced Subtidal Flat

Description

FA3 constitutes the thickest vertical accumulation of sandstone deposits in this study and appears tabular across the 12-km-long studied outcrop. It accommodates two types of very fine to fine-grained sandstones; one is well sorted and the other is moderately sorted. They interbed (Figure 4) and form up to 8-m-thick bedsets. At Cerro Pampa Tril, two genetically separate bedsets are stacked together to form a ca. 15-m-thick composite bedset. The moderately sorted sandstones dominate FA3 and are found across the entire study area. The well-sorted sandstones are found in highest concentration at Cerro Pampa Tril and Barranca Los Loros localities.

The clean, well-sorted sandstones (Figure 4, yellow color) comprise HCS (Facies G), swaley (SCS) (Facies H) (Figure 2F), low-angle (LaCS) (Facies I), and trough cross-stratification (Facies J) (Figure 2G), with sporadic *Thalassinoides*, *Gyrochorte*, and *Ophiomorpha* trace fossils (BI 1-2). LaCS occurs only at Cerro Pampa Tril. Beds are 10- to 50-cm-thick, and their sharp, flatly to gently undulating erosional bases exhibit <30-cm relief. Bed tops are either in sharp erosional contact with or grading into the moderately sorted muddy sandstones (Figure 5).

The muddy, moderately sorted sandstones (Figure 4, brown color) contain trough cross-stratification with reactivation surfaces (*sensu* Klein, 1970) and herringbone structures (Facies K) (Figures 2H–J); asymmetric and combined flow ripple (Facies L) (Figures 2K,L), bundled symmetric ripple (Facies M), and climbing ripple cross-lamination (Facies N); lenticular, wavy, and flaser bedding (Facies O–Q) (Figures 2M–O); and structureless and intensively bioturbated sandstone beds (Facies R–S). Paleocurrent reconstructions (included in Figure 1D) at Cerro Pampa Tril ($n = 10$) and Barranca Los Loros ($n = 19$) mainly support deposition by NE–SW bidirectional currents, with

dominance toward southwest, with subsidiary measurements that record other directions (Figure 1D). Measurements from Pampa Tril ($n = 7$) and Río Pequenco ($n = 25$) sections indicate deposition by NW–SE bidirectional currents, with dominance toward northwest, and a few measurements go in other directions (Figure 1D). *Thalassinoides*, *Gyrochorte*, and *Ophiomorpha* trace fossils are abundant (BI 3–6), whereas *Spongeliomorpha* and *Palaeophycus* (Figure 3D) are found at Pampa Tril (BI 3) and *Arenicolites* (Figure 3H) is found at Cerro Pampa Tril (BI 2). Beds are 20- to 50-cm thick, and their bases are either sharp-flat erosional or gradually overlying the clean sandstones. Bed tops are in sharp erosional contact with overlying strata.

Interpretation

FA3 reflects sand-rich subtidal flat deposits, which at places preserve interbedded storm-influenced deposits. This interpretation derives from the abundance of tidal process indicators across the studied section, the lateral extent, dimensions, and tabular appearance of the succession and its relationship to neighboring stratigraphic units. HCS and SCS beds were formed by storm waves (Harms et al., 1975; Leckie and Walker, 1982; Duke, 1985). HCS typically grades shoreward into SCS sandstone deposits in the middle shoreface, due to the increased wave energy (Leckie and Walker, 1982). Seen in stratigraphic context, LaCS at Cerro Pampa Tril is also interpreted to belong to the lower to middle shoreface environment, deposited from intense storm wave activity in conditions similar to upper oscillatory regime (Arnott, 1993). Only minor preservation of fair-weather wave structures occurs in FA3, represented by combined flow ripples and bundled symmetric ripples, even though these structures could also have formed from lesser wave energy in the waning of storms.

Bidirectional current measurements from the moderately sorted sandstones (Facies K–L) (Figures 1D, 2H and Table 1) reflect systematic current reversals and indicate that the cross-strata truly migrate in opposite directions and that this is not just an artificial effect of measurements of trough cross-stratification. Climbing ripples suggest rapid deceleration of current flow velocity and associated rapid deposition of suspended load material (Facies N and Table 1) (Allen, 1973; Nichols, 2009, p.53). Abundancy in lenticular, wavy, and flaser bedding (Facies O–Q), with double and single mud drapes, testify of alternations of flowing and standing water conditions. These sedimentary structures infer a depositional environment that was dominated by flowing currents and current reversals. Combining this interpretation with a marine trace fossil assemblage suggests that the moderately sorted sandstones were deposited in a tide-influenced environment. In this context, double mud drapes point toward a subtidal environment, where mud draping occurred at both high and low tide. The overall extensive bed tabularity reflects that these deposits accumulated in a subtidal flat environment. Some of the combined flow ripples are interpreted to represent reworking of unidirectional current ripples during current reversals (Dumas et al., 2005). Presence of climbing ripples are not definitive or characteristic for a specific depositional environment; they are widespread in fluvial and turbidity current deposits (Allen, 1973 and the references

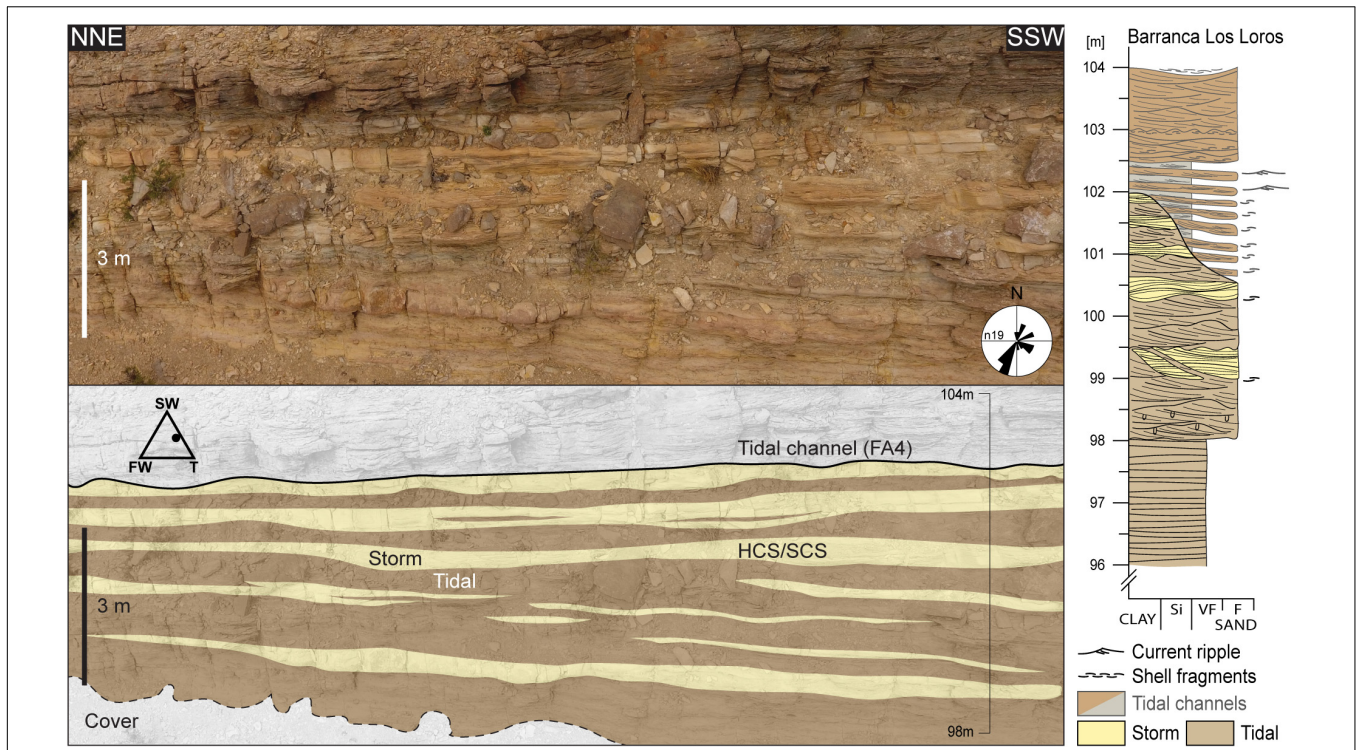


FIGURE 4 | Panel overview of FA3 facies arrangement at Barranca Los Loros (Figure 1D) and the corresponding sedimentary log. Figure location indicated in Figure 9. Storm deposits comprise HCS (Facies G) and SCS (Facies H) sandstones, while bimodal current indicators, reactivation surfaces, and single- and double-mud drapes define the heterogeneous tidal sandstones. Paleocurrent measurements and ternary diagram bedset plot included (modified from Dashtgard et al., 2012). SW, storm wave; FW, fair-weather wave; T, tide.

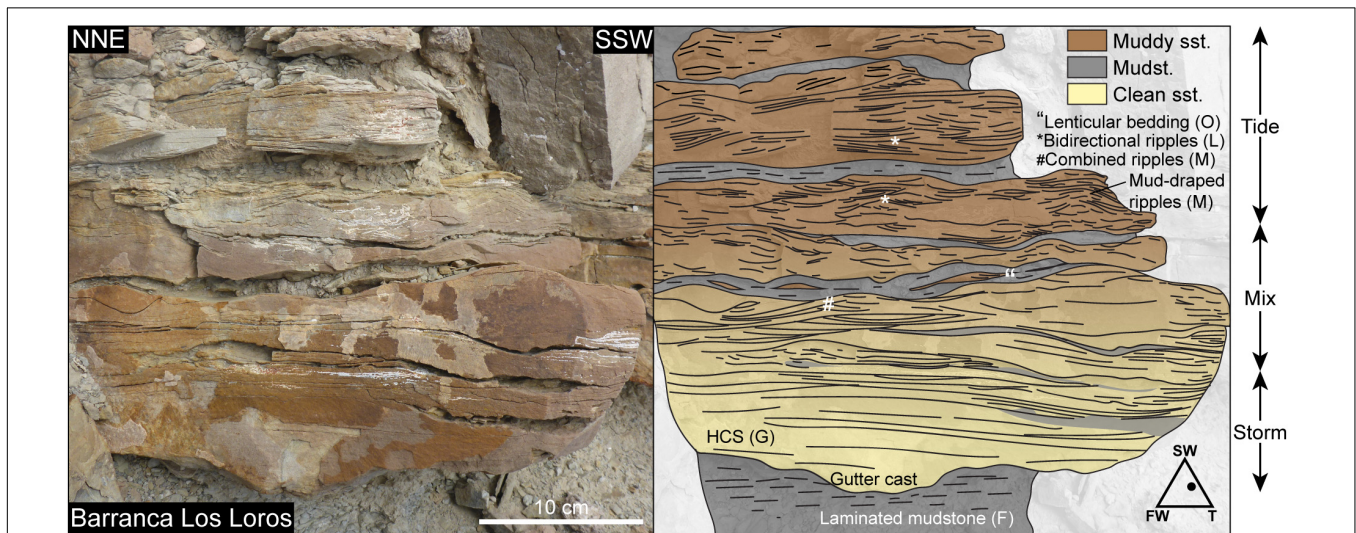


FIGURE 5 | Facies transition recorded at Barranca Los Loros (Figure 1D). Figure location is indicated in Figure 9. Gradual transition from storm (yellow) to tidal (brown) deposits, shown by original picture (left) and overlay interpretation (right). Yellow color corresponds to clean HCS sandstone (Facies G), brown color represents muddy sandstone, and gray color reflects laminated mudstone (Facies F); bracketed letters refer to Facies ID (cf. Table 1), ternary diagram bedset plot included (modified from Dashtgard et al., 2012); SW, storm wave; FW, fair-weather wave; T, tide.

therein), but they are also common in association with tidal dynamics on a tidal flat or lagoon environment (Yokokawa et al., 1995; Lanier et al., 1998). The paleocurrent reconstructions from

each locality show that some measurements go in directions at an angle to the measured bidirectionality, especially at Río Pequenco (Figure 1D). These particular paleoflow directions

are interpreted to reflect influence from longshore currents and fair-weather waves along the subtidal flat.

Interbedding and the erosional contacts between storm- and tide-influenced deposits reflect process interaction and their capacity to remobilize each other's deposits (as documented by, e.g., Rossi and Steel, 2016; Van Cappelle et al., 2016, 2017; Wei et al., 2016). The documented gradual transitions from storm into tidal deposits upward (**Figure 5**) are interpreted to represent the ability for tides to gradually regain relative dominance for sediment reworking in the aftermath of storm events.

FA4—Tidal or Tide-Influenced Channels

Description

FA4 is the coarsest (fine- to medium-grained sand) and most competent, ledge-forming unit in the study area, but it does also comprise some easily weathered heterolithics. Facies included in FA4 are laminated mudstones (Facies F), trough cross-stratified sandstones with shell gravel and abundant reactivation surfaces (Facies K), asymmetric ripple (Facies L) and climbing ripple cross-laminated sandstones (Facies N), and wavy- and flaser-bedded sandstones (Facies P–Q). Single and double mud-drapes are widespread in the sand-dominated facies, while basal shell gravel within trough cross-stratified sandstones (Facies K) is most abundant at the base of FA4, and the facies grades upward into better sorted, fine-grained sandstones. FA4 varies in lateral extent from a few tens of meters and up to *ca.* 8 km. The top bounding surface of FA4 is sharp-flat, while the base bounding surface caps FA3 by a sharp, flatly to gently inclined erosive base. At Barranca Los Loros (**Figure 6**), and 1 km south (**Figure 7**), a total of seven erosive FA4 units are recorded, with a concave-up erosional base, on top of FA3 deposits. These erosive features belong to the same stratigraphic unit, are 30- to 100-m wide (**Figures 6A, 7A**), exhibit up to 5-m erosional relief (**Figures 6A', 7B**), cut FA3 deposits by a sharp erosional contact (**Figure 7C**), and carve into FA3 well-sorted HCS (Facies G) (**Figure 7D**) and moderately sorted sandstones. FA4 strata are at places organized in gently inclined heterolithic strata (IHS) (*sensu* Thomas et al., 1987) (see log in **Figure 4**, and photos in **Figures 6B,C**), located next to the concave-up erosive features. The IHS comprise up to 10-cm-thick individual layers of asymmetric ripple-laminated sandstones with mud-drapes (Facies L), which are interbedded with laminated mudstones (Facies F) (**Figure 6B**) and resemble wavy-bedded heterolithics (Facies P). Orthorectified photos from VOMs reveal that these deposits dip with a *ca.* 5° angle to the underlying bedding surface of FA3 deposits (**Figure 6C**), following the orientation of the down-cutting erosive features described above (**Figures 6A',C**). The contact between the IHS and the underlying FA3 deposits appears to be conformably gradual at some places (**Figure 6C**) and otherwise sharply erosional (log in **Figure 4**).

Interpretation

FA4 records meandering subtidal channel deposits. The interpretation of FA4 as tide-influenced is threefold, starting with the sedimentary composition. The sedimentary facies assemblage reflects that FA4 was mainly deposited by flowing currents. The heterolithic components of wavy bedding and IHS indicate that there was a systematic alternation between

flowing and quiescent water conditions, and the abundance of mud-drapes in the sand-dominated facies (ripple-laminated and flaser-bedded sandstones) reveal periodic mud-draping during the quiescent water conditions. Abundance of shell gravel in the troughs of FA4 trough cross-stratified sandstones places the deposits in a marginal marine environment. Reactivation surfaces are representative of subtidal environments, but if they are not cyclically distributed they may also originate from fluvial streams (Gugliotta et al., 2016 and the references therein). The sedimentary facies assemblage can be explained in two ways: FA4 was deposited under conditions of tidal currents or under the influence from a fluvial system that experienced seasonal discharge variations.

Looking at the architectural elements, the seven concave-up erosive features are interpreted to represent channel-shapes, meaning that the contained FA4 strata reflect channel deposits. The orthorectified drone photos in **Figures 6A', 7A'** show that the channels cut the underlying FA3 deposits with an angle that approximates oblique to perpendicular to the outcrop orientation, as both sides of the channels are exposed in the outcrop transect. The IHS neighboring the channels (**Figures 6A',C**) are considered to be evidence of lateral accretion surfaces, from channel and bar migration, as they follow the orientation and dip of the channel bases. In modern and ancient systems, lateral accretion surfaces that are organized in IHS are found throughout tide-dominated channels and fluvial-dominated channels with seasonal discharge (Thomas et al., 1987; Sisulak and Dashtgard, 2012 and the references therein).

Considering the stratigraphic context, most contacts between FA3 and FA4 are erosional, meaning that possible base level changes between the two units cannot be completely ruled out. However, even though a sharp erosional contact between FA3 and FA4 deposits may be concealed within the finer-grained IHS at Barranca Los Loros (**Figure 6C**), the seemingly conformable and gradual transition suggests that FA3 and FA4 are genetically related, preserving continuous sedimentation across the transition, which suggests that there is no substantial time-gap or base-level change. Given the subtidal setting for FA3 deposits, it is considered most appropriate to their genetic relation that the systematic current energy variations recorded in FA4 are linked to tidal influence on deposition at a subtidal position, similar to the conditions that formed FA3. However, whether or not these channel deposits were disconnected from a potentially fluvial sediment feeder system further inland remains unknown, as there is no known data or published material on the landward extent of the upper Mulichinco Fm. in the area.

FA5—Ooid Bars or Dunes With Bioclastic Shell Fragments

Description

FA5 records 1- to 5-m-thick tangential to sigmoidal cross-stratified oolitic grainstone with shell fragments (Facies E). FA5 is exclusive to Cerro Pampa Tril and caps FA3 deposits by a sharp, undulating, and erosional contact, which exhibits up to 6 m of erosional relief (**Figure 8**). Its extent in outcrop limits to *ca.* 370-m width and *ca.* 6-m thickness. VOMs reveal that

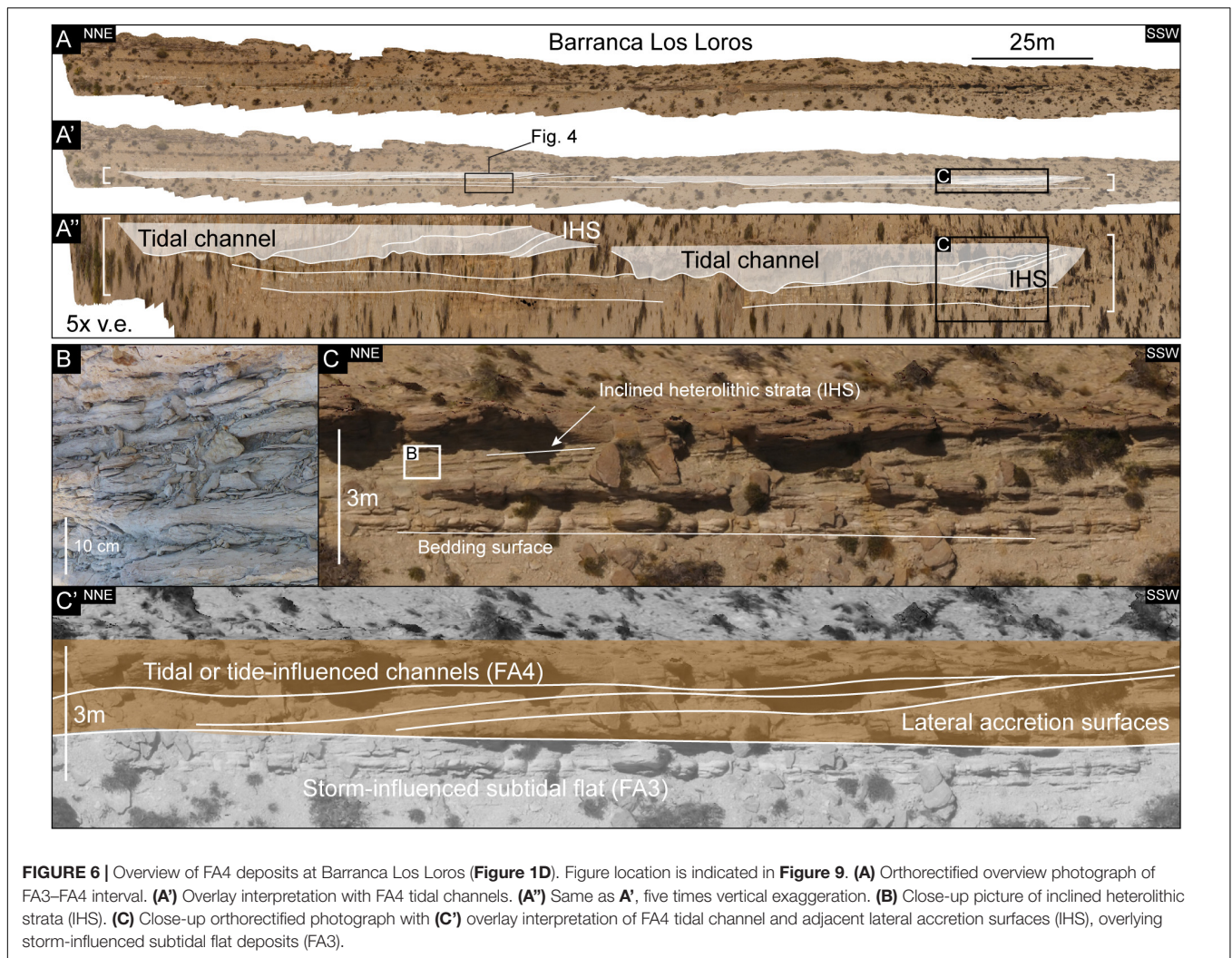


FIGURE 6 | Overview of FA4 deposits at Barranca Los Loros (Figure 1D). Figure location is indicated in Figure 9. (A) Orthorectified overview photograph of FA3–FA4 interval. (A') Overlay interpretation with FA4 tidal channels. (A'') Same as A', five times vertical exaggeration. (B) Close-up picture of inclined heterolithic strata (IHS). (C) Close-up orthorectified photograph with (C') overlay interpretation of FA4 tidal channel and adjacent lateral accretion surfaces (IHS), overlying storm-influenced subtidal flat deposits (FA3).

FA5 cross-strata are amalgamated and erosively based (Figure 8). Cross-set thicknesses range between 1 and 5 m (Figures 8B,C), the thickest of which contains sigmoidal foresets (Figure 8C). Paleocurrent measurements ($n = 10$) from one of the cross-sets (Figure 8B) indicate unidirectional flow toward southwest.

Interpretation

FA5 reflects ooid bars or compound dunes with bioclastic shell fragments. This interpretation is driven by the thick dimensions and complex dune-like geometry of the cross-strata, resembling the compound bioclastic dunes of Olariu et al. (2012) and is strengthened by the stratigraphic context of a subtidal environment in FA3. FA5 could also be the outcrop expression of the up to 4-m-thick oolitic-skeletal grainstone-packstone facies of Schwarz et al. (2016), which were identified from subsurface core material alone, approximately 45 km northeast of Pampa Tril (this study). Schwarz et al. (2016) interpreted these deposits to represent ooid shoals that formed above a fair-weather wave base. However, as the cross-set thicknesses were described as less than 60 cm, the FA5 deposits may be of a different origin. The 1- to 5-m-thick cross-sets of FA5 (Figures 8B,C) indicate

water depths of 5 m minimum, whereas the deposits of Schwarz et al. (2016) formed in at least 0.6 m water depth. Ooids form in high-energy environments, above a fair-weather wave base (Reeder and Rankey, 2008 and the references therein), but the stratigraphic context of a subtidal environment in FA3 may suggest that the ooids and shell fragments in FA5 were reworked and transported onto the subtidal flat and deposited as compound dunes.

Correlation and Outcrop Orientation

Correlation across the study area is based on confident visual tracing of surfaces and strata from VOMs that cover the study area. Eight regional flooding surfaces (FSs) (*sensu* Catuneanu et al., 2009), which separate high-frequency stratigraphic sequences (Schwarz, 2012; Schwarz et al., 2013, 2016), are used as correlative markers (Figure 9) and treated as sequence boundaries for this study. A higher order maximum regressive surface (MRS) (*sensu* Helland-Hansen and Martinsen, 1996) is identified toward the top of the most regressive sequence, located between FS6

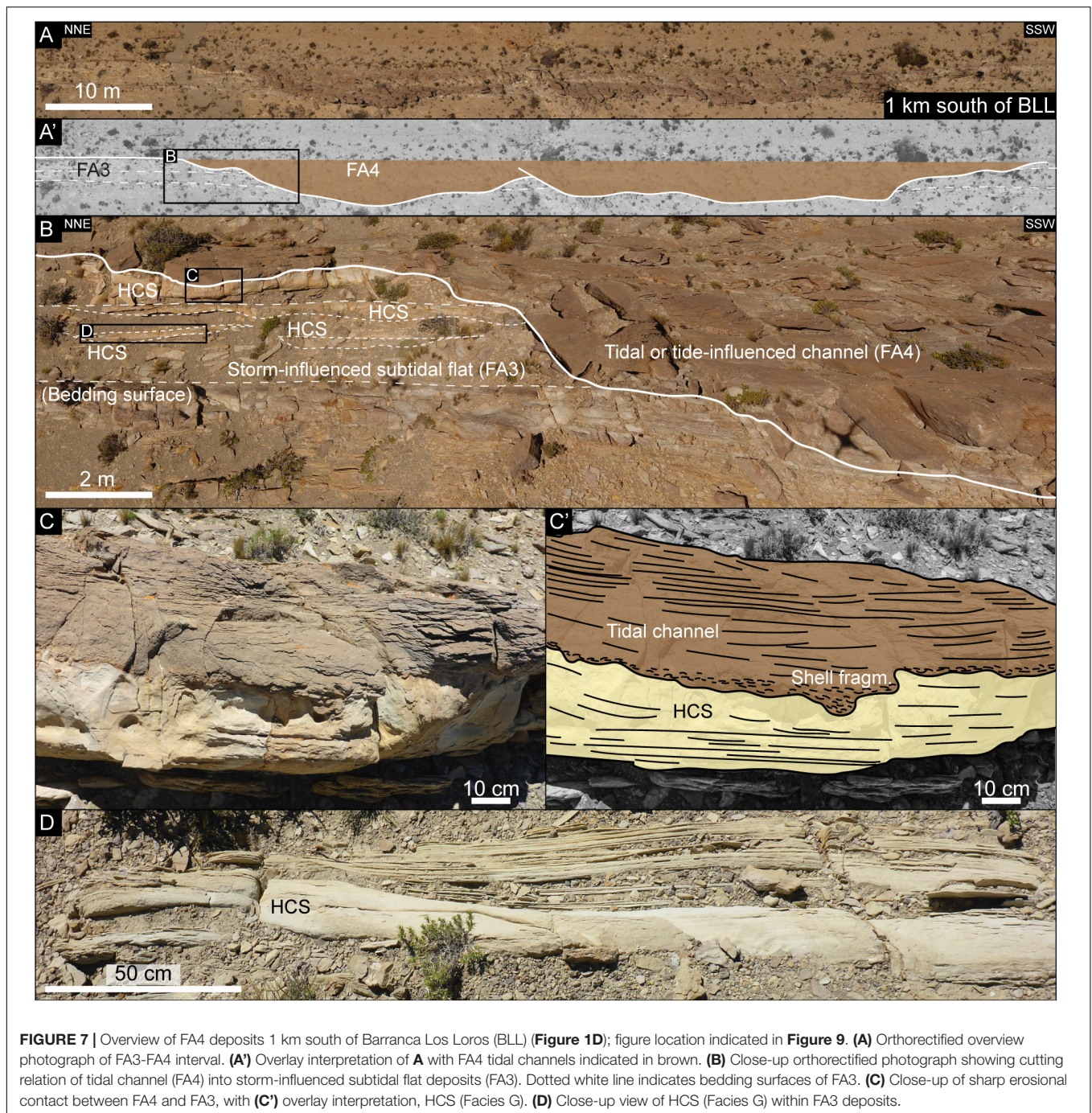


FIGURE 7 | Overview of FA4 deposits 1 km south of Barranca Los Loros (BLL) (**Figure 1D**); figure location indicated in **Figure 9**. **(A)** Orthorectified overview photograph of FA3-FA4 interval. **(A')** Overlay interpretation of **A** with FA4 tidal channels indicated in brown. **(B)** Close-up orthorectified photograph showing cutting relation of tidal channel (FA4) into storm-influenced subtidal flat deposits (FA3). Dotted white line indicates bedding surfaces of FA3. **(C)** Close-up of sharp erosional contact between FA4 and FA3, with **(C')** overlay interpretation, HCS (Facies G). **(D)** Close-up view of HCS (Facies G) within FA3 deposits.

and FS7 (**Figures 9, 10**) and completes the correlative surface framework.

The main target for this study is located between FS5 and MRS (**Figures 9, 10**), which represents the most sand-rich part of the upper Mulichinco Fm. This succession highlights subtidal flat complexes (FA3), tidal channel-fills (FA4), and ooid bars or dunes (FA5). Spatial distribution of interbedded storm and tidal deposits of FA3 vary significantly, with the relative presence of storm deposits varying from 60 to 0% (**Figure 10**). Storm deposits are thickest and most abundant at Cerro Pampa Tril and

Barranca Los Loros, while thinner or absent at Pampa Tril and Río Pequenco localities. Distribution of these interbedded storm deposits defines 3.5 km wide and <8 m thick lensoids (**Figure 10**), as expressed in the outcrop.

High-frequency FSs within the upper Mulichinco Fm. help constrain sedimentary architecture of genetically-related stratigraphic units (**Figure 10**). At Río Pequenco (**Figure 10**), FS5.3 forms an apparent NW-dipping clinoform, interpreted to represent the northern extent of the underlying subtidal flat complex. The remaining FSs and stratigraphic units appear

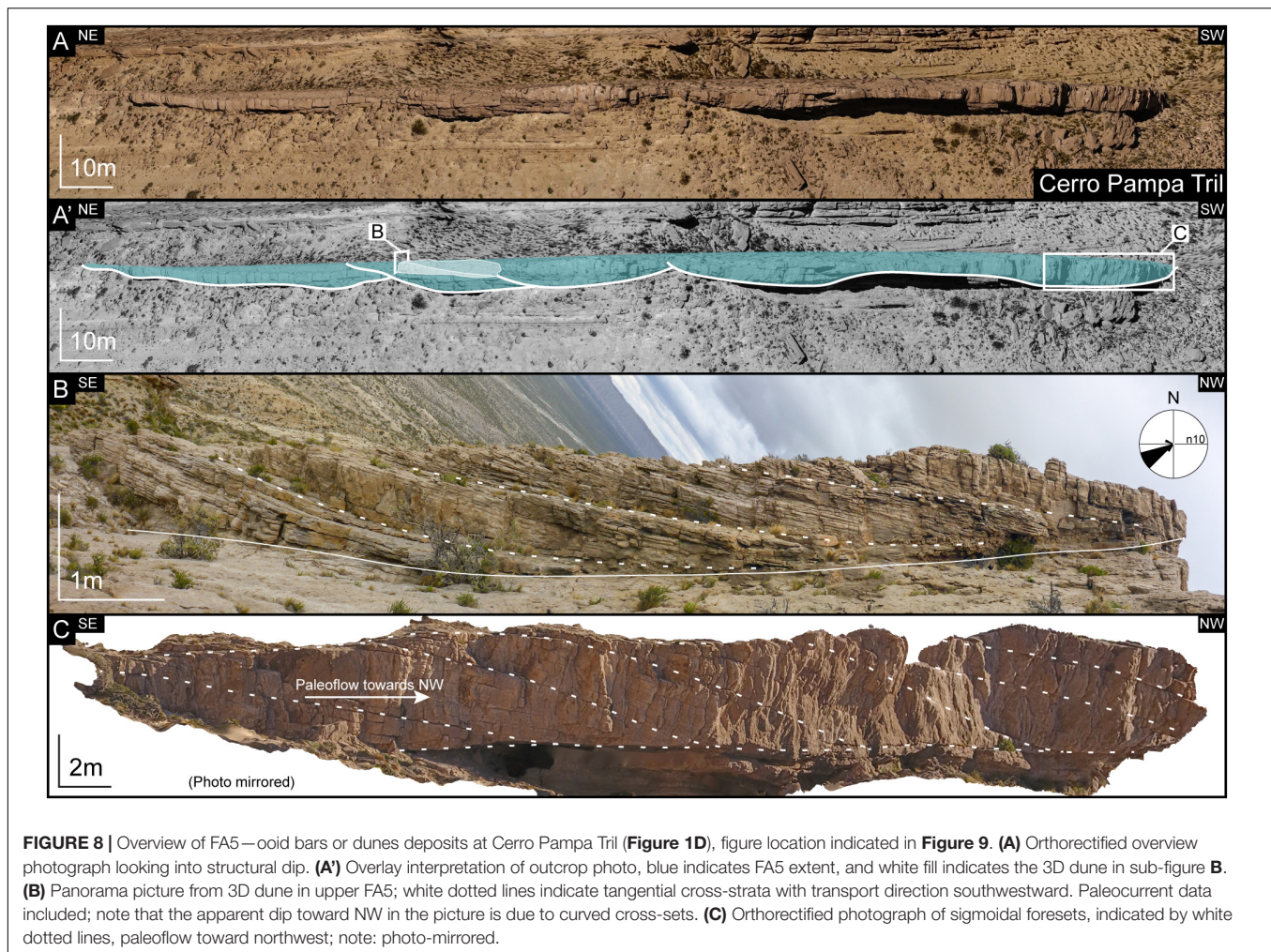


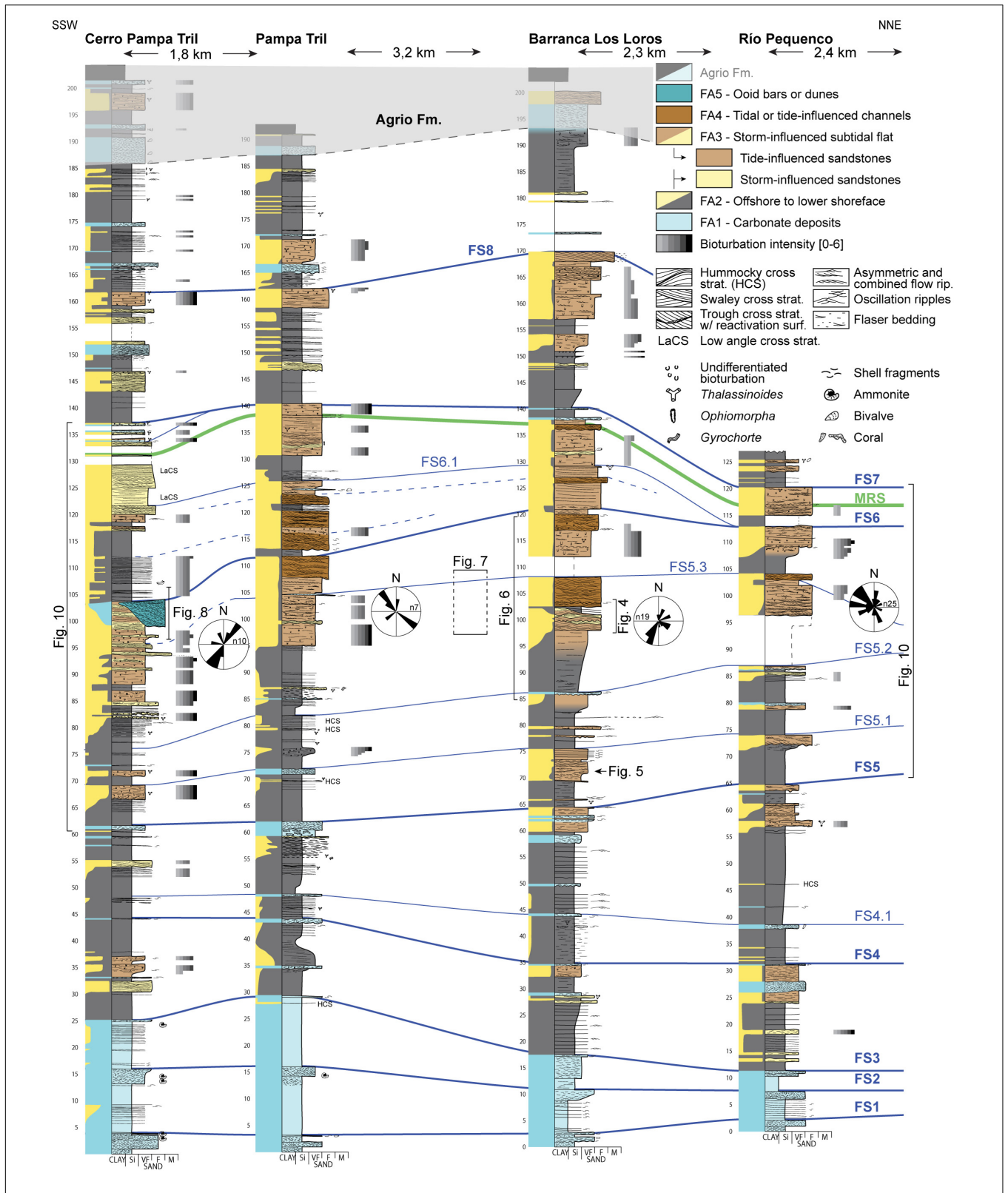
FIGURE 8 | Overview of FA5—oid bars or dunes deposits at Cerro Pampa Tril (Figure 1D), figure location indicated in Figure 9. (A) Orthorectified overview photograph looking into structural dip. (A') Overlay interpretation of outcrop photo, blue indicates FA5 extent, and white fill indicates the 3D dune in sub-figure B. (B) Panorama picture from 3D dune in upper FA5; white dotted lines indicate tangential cross-strata with transport direction southwestward. Paleocurrent data included; note that the apparent dip toward NW in the picture is due to curved cross-sets. (C) Orthorectified photograph of sigmoidal foresets, indicated by white dotted lines, paleoflow toward northwest; note: photo-mirrored.

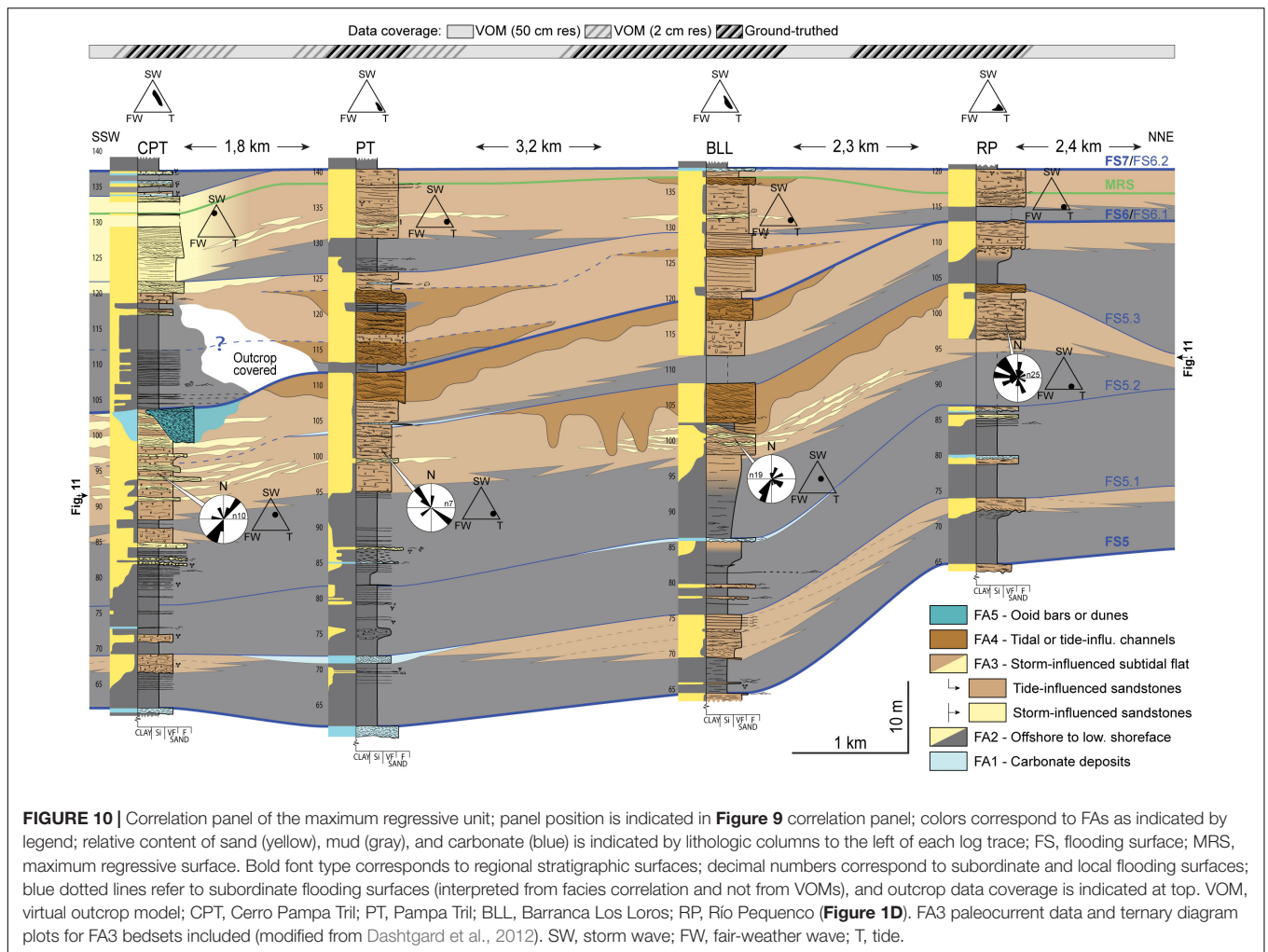
otherwise tabular across the studied NNE- to SSW-striking outcrop. Additionally, as no consistent facies change is recorded across the outcrop, we consider the outcrop to be oriented sub-parallel to the paleocoastline, primarily showing along-strike variability of its deposits.

Paleocoastline and Sedimentary Environment

Several previous studies suggest that the upper Mulichinco Fm. sedimentary succession is a product of systematic fluctuations in relative sea level on a low-gradient ramp, where carbonate production (FA1 and FA5) dominated the transgressive phases and siliciclastic deposition (FA2, 3, and 4) dominated the regressive phases (Schwarz, 2012; Schwarz et al., 2013, 2016). This study focuses on the mixing of storm- and tide-influenced siliciclastic deposits in FA3, and the reconstruction of sedimentary environment is hence centered on the siliciclastic-dominated stages of the upper Mulichinco Fm. Consequently, this contribution does not further discuss the sedimentary environments of the carbonate-dominated development stages (FA1 and FA5).

Schwarz and Howell (2005) recorded a basinward facies change toward the northwest in the upper Mulichinco Fm. and placed the associated N–S-oriented paleocoastline east of the Pampa Tril area of this study (Figure 11A). As the paleocurrent dataset of this study (Figures 1D, 10) exhibits bidirectionality with dominant paleocurrent directions toward northwest and southwest, away from the paleocoastline of Schwarz and Howell (2005), we propose that the coastal system was dominated by ebb-tidal currents. Additionally, this documented variation in paleocurrent directions of FA3 is considered as evidence of deposition along an irregular paleocoastline, consisting of protrusions and bays (Figure 11B). These coastal morphologies directly affected wave and tidal process distributions and interactions through wave refraction (Figure 11C). With an expected increased wave energy at coastal protrusions (Swift and Thorne, 1991), the relatively higher abundance of storm deposits at Cerro Pampa Tril and Barranca Los Loros (Figures 1D, 10) suggest that paleocoastal protrusions were positioned close to these localities (Figures 11C,D). Accordingly, lower abundance and absence of storm deposits at Pampa Tril and Río Pequenco suggest that the paleoenvironments of these localities experienced weaker wave energy, which is expected in embayments.





The sedimentary environment (**Figure 11B**) consisted of offshore to lower shoreface siliciclastics (FA2), storm-influenced subtidal sand flat complexes (FA3), and neighboring tidal channels (FA4). Storm- and tide-influenced deposits mix spatially on bed- (**Figure 5**), bedset- (**Figure 4**), and high-frequency sequence scales (**Figure 10**). In other words, the upper Mulichinco coastal and inner shelf environment experienced multi-scale interaction between storm waves and tides. However, the tide-influenced deposits are prevalent across the outcrop, suggesting that the tidal currents were persistent, while storm-influence was erratic and common only at specific localities. Mapping of landward facies, such as intertidal and supratidal/continental/fluvial equivalents, is impossible, as there is no known data or published material on these deposits adjacent to the study area.

DISCUSSION

Sediment Dispersal and Process Mixing

Cerro Pampa Tril and Barranca Los Loros localities (**Figure 1D**) were located close to coastal protrusions (**Figure 11B**), where

efficient convergence of wave energy favored local storm influence along the subtidal flat environment (**Figures 10, 11C**). Between these protrusions, embayments decreased wave energy, favoring complete tidal remobilization of wave-influenced deposits at Pampa Tril and Río Pequenco localities (**Figures 1D, 10, 11C,D**). Interplay between waves and tides was in this way governed by the dispersal of wave energy along the irregular paleocoastline.

Understanding of wave and tidal process distribution in the upper Mulichinco Fm. can be graphically visualized by plotting its deposits onto ternary diagrams. As there are no definitive fluvial structure recorded/preserved in this study, the ternary diagram from Dashtgard et al. (2012) is considered most useful to apply, as it allows for distinguishing between the relative contribution of fair-weather and storm waves and tides. **Figures 4, 5, 10, 11D** include several of such ternary diagrams, together expressing the variability in relative contribution of wave and tidal processes on bed-scale (**Figure 5**), bedset-scale (**Figure 4**), and between localities (FA3 and bulk locality plots in **Figures 10, 11**). Combined, these plots can graphically visualize the process heterogeneity in the study area, not as a single point, but contoured to simultaneously show relative dominance and

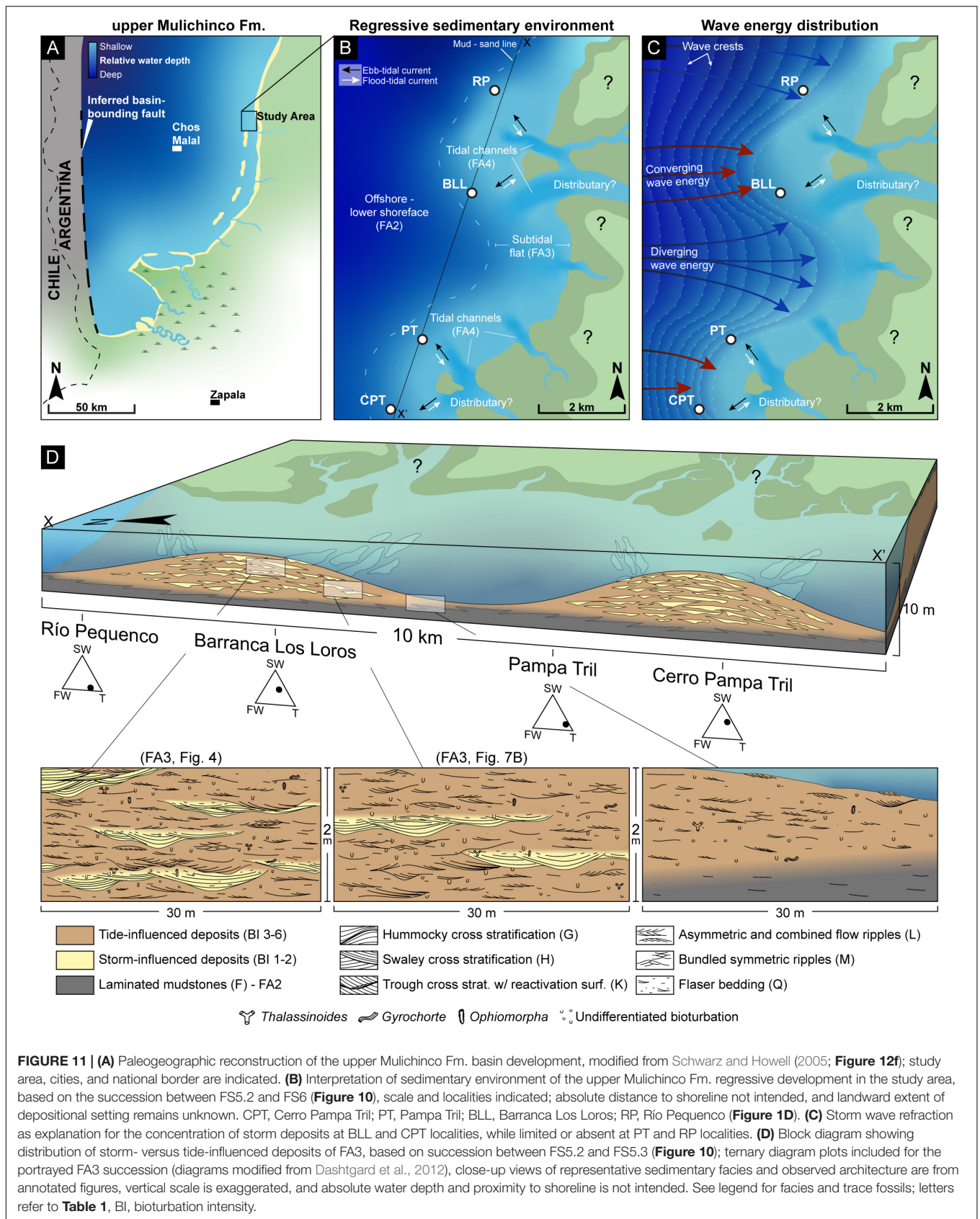
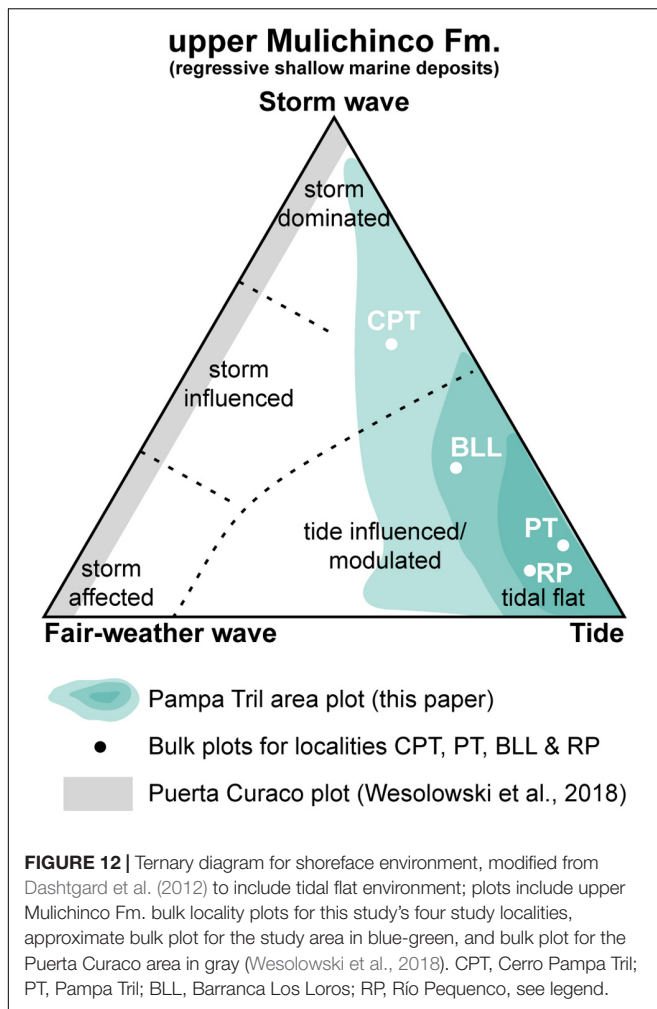


FIGURE 11 | (A) Paleogeographic reconstruction of the upper Mulichinco Fm. basin development, modified from Schwarz and Howell (2005; **Figure 12f**); study area, cities, and national border are indicated. **(B)** Interpretation of sedimentary environment of the upper Mulichinco Fm. regressive development in the study area, based on the succession between FS5.2 and FS6 (**Figure 10**), scale and localities indicated; absolute distance to shoreline not intended, and landward extent of depositional setting remains unknown. CPT, Cerro Pampa Tril; PT, Pampa Tril; BLL, Barranca Los Loros; RP, Río Pequenco (**Figure 1D**). **(C)** Storm wave refraction as explanation for the concentration of storm deposits at BLL and CPT localities, while limited or absent at PT and RP localities. **(D)** Block diagram showing distribution of storm- versus tide-influenced deposits of FA3, based on succession between FS5.2 and FS5.3 (**Figure 10**); ternary diagram plots included for the portrayed FA3 succession (diagrams modified from Dashtgard et al., 2012), close-up views of representative sedimentary facies and observed architecture are from annotated figures, vertical scale is exaggerated, and absolute water depth and proximity to shoreline is not intended. See legend for facies and trace fossils; letters refer to **Table 1**, BI, bioturbation intensity.



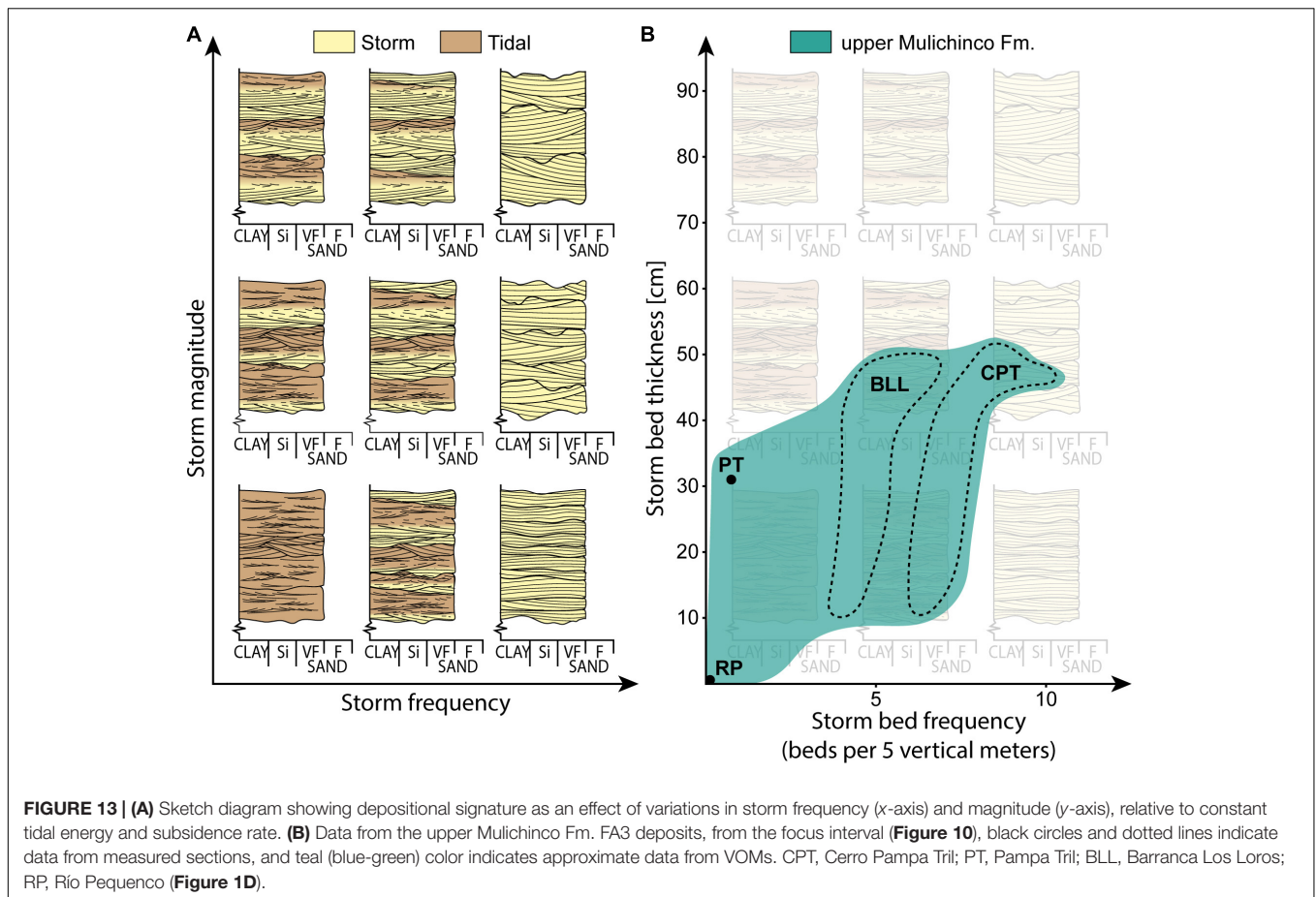
variability (Figure 12). These approximate plots indicate storm dominance and tide-influence at Cerro Pampa Tril and Barranca Los Loros, and tide-dominance at Pampa Tril and Río Pequenco (Figures 10, 11D, 12).

The dataset exhibits a gently increased storm wave dominance toward southwest (Figure 10). Cerro Pampa Tril records the thickest accumulation of mixed wave- and tide-influenced deposits (between FS5.2 and FS6, Figure 10) and accommodates the highest concentration of storm deposits of this study (between FS6.1 and FS6.2; Figure 10). Wesolowski et al. (2018) described the upper Mulichinco Fm. deposits at Puerta Curaco (Figure 1C), a locality *ca.* 20 km southwest of this study. Their results show a succession that was deposited in a higher energy setting, governed by storm and fair-weather wave reworking. Meters-thick amalgamated HCS and SCS deposits, and a generally much-better sorted succession than the one documented in this study, were reported from the same study. Wesolowski et al. (2018) further identified upper shoreface deposits, which arguably positions the locality marginally closer to the shoreline than the deposits documented in this study. Nevertheless, Wesolowski

et al. (2018) concluded that Puerta Curaco was entirely wave-dominated (non-tidal) and did not identify any sign of tidal influence (Figure 12). In light of their findings, and the southwestward increase in wave energy documented in this study, we suggest that the upper Mulichinco Fm. represents a coastal system that experienced both spatial differences in relative process dominance, on regional and local scales, and dynamic interaction of wave and tidal processes on local scale; overall, wave processes dominated in the Puerta Curaco area (Wesolowski et al., 2018) while tides dominated in the Pampa Tril area (this paper).

Similar to the FA3 deposits of this study, Wei et al. (2016) documented facies relations within the Rannoch Fm., Northern North Sea. Their study was based on core data and showed that the Rannoch Fm. exhibits a successive alternation of erosive storm and tidal deposits in a lower to middle shoreface setting. Wei et al. (2016, Figure 9) developed a schematic depositional model to explain how waves and tides efficiently remobilized sediments and successively replaced each other's roles as dominant modification processes. Their model relies on a fluvial source for sediment transport. However, waves and tidal currents are capable of remobilizing and transporting sediments along the coastline, through, e.g., swash and longshore currents, storm-related processes, and tidal currents. Even though they are thought of as modification processes, waves and tidal currents may in this way act as the only sediment transport agents to coastal environments neighboring a deltaic system (Swift and Thorne, 1991; Legler et al., 2014), so that these environments may not contain any signs of fluvial influence.

The landward extent of the sedimentary paleoenvironment, and thereby the driving mechanisms behind the creation of the proposed irregular paleocoastline, remain unknown. However, fluvial, wave, and tidal processes were responsible for the paleocoastal morphology, as long as there were no substantial differences in lithology that would naturally make the waves erode the paleocoastline irregularly. Waves tend to smooth and straighten coastlines (e.g., Boyd et al., 1992), meaning that the paleocoastal protrusions of the upper Mulichinco Fm. were constructed and maintained by tidal and/or fluvial processes, which brought sediments into the basin. Both fluvial and tidal channels construct protruding mouth bars (modern examples in Allen, 1970; Allen and Mercier, 1994), which at an early stage represent subaqueous protrusions that converge waves and provide excellent sources for sand to be reworked by both waves and tidal currents. The presence of a fluvial sediment feeder system remains undocumented for this study, but as braided and meandering fluvial continental deposits have been evidenced from the lower Mulichinco Fm. outcrops (Schwarz and Howell, 2005; Schwarz et al., 2006), it is relevant to consider that a similar fluvial system could have been active during deposition of the upper Mulichinco Fm. as well. From the aforementioned arguments, the sand-rich FA3 storm deposits are interpreted to have been reworked at or near channel mouths (as illustrated in Figure 11). The FA4 tidal or tide-influenced channels at Barranca Los Loros (Figure 10) further strengthen this interpretation, as they are situated directly on top of storm-influenced deposits. Both waves and tidal currents



further dispersed sand along the paleocoastline, away from the channel mouths, and into the bays.

From the lack of any definitive fluvial deposits, the measured sections of this study appear to have developed in positions too far removed from fluvial influx points for this to have directly affected the preserved stratal architecture. Based on the presented data, ebb-tidal current dominance is therefore suggested to have been the main driver for sediment dispersal and progradation onto the subtidal flat environment (FA3) through meandering tidal channels (FA4). This observed ebb-tidal current dominance could be the result of a fluvial system inland that helped transport the sediments in a basinward direction; but this remains unknown. The preserved mixed-process deposits were hence entirely governed by the interaction of waves and tides, and even if a potential fluvial system did influence on stratal architecture, all fluvial traces were overprinted.

Preservation Potential

As mixed coastal processes successively alter sediment sorting, textures, internal structures, and distribution through time and space, the preserved sedimentary deposits are only products of the last processes that acted on the sediments before lithification. The sediments may thus have been reworked several times before preservation, meaning that the lack of signals from

a certain process is not a definite evidence for its absence during deposition.

Understanding how different basin-specific parameters affected deposition helps constrain what factors influenced on preservation. For the studied upper Mulichinco Fm., subsidence rate and distribution of depositional and modification processes (tidal energy and storm frequency/magnitude) are the known parameters that directly affected preservation. Subsidence rate is impossible to constrain from this dataset and is therefore considered constant. Tidal energy is also considered constant. As the studied succession is a product of the interaction of episodic storms and persistent tides along an irregular paleocoastline, the distribution of wave energy is considered a major control on its preservation. Due to wave refraction, the upper Mulichinco Fm. shows that the potential to preserve storm-influenced deposits within a tide-dominated succession is relatively high along an irregular coastline, but it depends on the relative interplay between tidal currents and waves.

Climatic changes of storm frequency and magnitude could have played a major part in giving the upper Mulichinco Fm. its depositional signature, but the result of wave refraction could potentially have overprinted/cluttered these climatic signals (Figure 13A). Near coastal protrusions, converging wave energy results in high wave impact frequency/magnitude, while diverging wave energy in deeper bays results in low wave impact

frequency/magnitude (Figures 11C,D, 13). Looking at the upper Mulichinco Fm. dataset (Figure 13B), the deposits from Pampa Tril and Río Pequenco localities (Figure 1D) exhibit few to no storm deposits in the focus interval (Figure 10); preservation at these localities compares to low storm frequency/magnitude relative to tidal energy (Figures 13A,B). As follows, for Cerro Pampa Tril and Barranca Los Loros localities (Figure 1D), thicker and higher abundance of storm deposits compare to an elevated storm frequency/magnitude (Figures 11D, 13A,B). Apparent temporal changes in storm frequency and magnitude may hence be attributed to wave refraction on paleomorphology and not solely due to syn-depositional climatic changes. Studies that target to reveal the true temporal changes in storm frequency and magnitude, based on the sedimentary composition of deposits alone, should therefore take this into account.

CONCLUSION

- The shallow marine depositional environment of the upper Mulichinco Formation comprises regional separation of wave and tidal process dominance and experienced a local dynamic interaction of waves and tides.
- Preservation of interbedded storm and subtidal flat deposits, as well as wave and tidal process distribution, interaction, and relative contribution were entirely governed by the effect of wave refraction along an irregular paleocoastline.
- Ebb-tidal currents dominated this tidal flat and channel complex and were the main intrabasinal driver for progradation and basinward siliciclastic sediment dispersal.
- The stratigraphic pattern in mixed storm and tidal deposits reflects the balance between continuous tidal deposition and intermittent disruptive reworking by storms.
- Several ternary diagrams can be combined to graphically explain spatiotemporal variability in relative process dominance in mixed-process coastal environments.

REFERENCES

- Ainsworth, R. B., Vakarelov, B. K., and Nanson, R. A. (2011). Dynamic spatial and temporal prediction of changes in depositional processes on clastic shorelines: toward improved subsurface uncertainty reduction and management. *AAPG Bull.* 95, 267–297. doi: 10.1306/06301010036
- Allen, J. R. L. (1970). "Sediments of the modern niger delta: a summary and review," in *Deltaic Sedimentation, Modern and Ancient*, eds J. P. Morgan and R. H. Shaver (Tulsa, OK: SEPM Society for Sedimentary Geology), 138–151. doi: 10.2110/pec.70.11.0138
- Allen, J. R. L. (1973). A classification of climbing-ripple cross-lamination. *J. Geol. Soc.* 129, 537–541. doi: 10.1144/gsjgs.129.5.0537
- Allen, G. P., and Mercier, F. (1994). "Reservoir facies and geometry in mixed tide and fluvial dominated delta mouth bars: example from the modern Mahakam delta (East Kalimantan)," in *Proceedings Indonesian Petroleum Association, IPA94-1.1-189, 23rd Annual Convention* (Jakarta), 261–273.
- Arnott, R. W. C. (1993). Quasi-planar-laminated sandstone beds of the Lower cretaceous bootlegger member, north-central montana; evidence of combined-flow sedimentation. *J. Sediment. Res.* 63, 488–494. doi: 10.1306/d4267b31-2b26-11d7-8648000102c1865d
- Bann, K. L., Fielding, C. R., MacEachern, J. A., and Tye, S. C. (2004). Differentiation of estuarine and offshore marine deposits using integrated ichnology and sedimentology: permian pebbly beach formation, sydney Basin, Australia. *Geol. Soc. Lon. Spec. Publ.* 228, 179–211. doi: 10.1144/gsl.sp.2004.228.01.10
- Boyd, R., Dalrymple, R., and Zaitlin, B. A. (1992). Classification of clastic coastal depositional environments. *Sediment. Geol.* 80, 139–150. doi: 10.1016/0037-0738(92)90037-R
- Buckley, S. J., Ringdal, K., Naumann, N., Dolva, B., Kurz, T. H., and Howell, J. A. (2019). LIME: software for 3-D visualization, interpretation, and communication of virtual geoscience models. *Geosphere* 15, 222–235. doi: 10.1130/ges02002.1
- Burton, D., Flaig, P. P., and Prather, T. J. (2016). Regional controls on depositional trends in tidally modified deltas: insights from sequence stratigraphic correlation and mapping of the Loyd and Segó Sandstones, Uinta and Piceance Basins of Utah and Colorado, U.S.A. *J. Sediment. Res.* 86, 763–785. doi: 10.2110/jsr.2016.48
- Catuneanu, O., Abreu, V., Bhattacharya, J. P., Blum, M. D., Dalrymple, R. W., Eriksson, P. G., et al. (2009). Toward the standardization of sequence stratigraphy. *Earth Sci. Rev.* 92, 1–33. doi: 10.1016/j.earscirev.2008.10.003

DATA AVAILABILITY STATEMENT

All datasets generated for this study are included in the article.

AUTHOR CONTRIBUTIONS

AS and IM led the research. AS wrote the manuscript and created the figures. All authors contributed to insightful discussions that formed this article and greatly improved the manuscript and figures. IM contributed significantly to the scientific progress of the research. AS, IM, and OG collected data. OG planned all necessary fieldwork logistics and located key research localities together with AS and IM in the field. HL provided knowledge on regional geology as well as detailed knowledge on the research target, and aided fieldwork planning and logistics.

FUNDING

The authors would like to thank AkerBP ASA for financial support. The funder was not involved in the study design, collection, analysis, interpretation of data, the writing of this article, or the decision to submit it for publication.

ACKNOWLEDGMENTS

The authors would like to thank Y-TEC and Octavio Palma for insightful discussions and fieldwork planning assistance. Special thanks are directed to Fredrik Wesenlund for assistance and great company during fieldwork. The authors would also like to direct their utmost gratitude to the reviewers SD, CO, and VR, and the associate editor DH, as well as Cari Johnson and Ernesto Schwarz who reviewed a previous version of this manuscript, for their extensive efforts and insightful comments that greatly improved the article.

- Clifton, H. E. (2006). "A reexamination of facies models for clastic shorelines," in *Facies Models Revisited*, eds H. W. Posamentier and R. G. Walker (SEPM Society for Sedimentary Geology), 293–337.
- Collins, D. S., Johnson, H. D., Allison, P. A., Guilpain, P., and Damit, A. R. (2017). Coupled 'storm-floor' depositional model: application to the Miocene-Modern Baram Delta Province, north-west Borneo. *Sedimentology* 64, 1203–1235. doi: 10.1111/sed.12316
- Dalrymple, R. (2010). "Tidal depositional systems," in *Facies Models 4*, eds N. P. James and R. Dalrymple (St. John's: Geological Association of Canada), 201–231.
- Dalrymple, R. W., Zaitlin, B. A., and Boyd, R. (1992). Estuarine facies models; conceptual basis and stratigraphic implications. *J. Sediment. Res.* 62, 1130–1146. doi: 10.1306/d4267a69-2b26-11d7-8648000102c1865d
- Dashtgard, S. E., Gingras, M. K., and MacEachern, J. A. (2009). Tidally modulated shorefaces. *J. Sediment. Res.* 79, 793–807. doi: 10.2110/jsr.2009.084
- Dashtgard, S. E., MacEachern, J. A., Frey, S. E., and Gingras, M. K. (2012). Tidal effects on the shoreface: toward a conceptual framework. *Sediment. Geol.* 279, 42–61. doi: 10.1016/j.sedgeo.2010.09.006
- Dean, C. D., Collins, D. S., van Cappelle, M., Avdis, A., and Hampson, G. J. (2019). Regional-scale paleobathymetry controlled location, but not magnitude, of tidal dynamics in the Late Cretaceous Western Interior Seaway, USA. *Geology* 47, 1083–1087. doi: 10.1130/g46624.1
- Donselaar, M. E. (1989). The Cliff House Sandstone, San Juan Basin, New Mexico: model for the stacking of 'transgressive' barrier complexes. *J. Sediment. Petrol.* 59, 13–27. doi: 10.1306/212F8F08-2B24-11D7-8648000102C1865D
- Duke, W. L. (1985). Hummocky cross-stratification, tropical hurricanes, and intense winter storms. *Sedimentology* 32, 167–194. doi: 10.1111/j.1365-3091.1985.tb00502.x
- Dumas, S., Arnott, R. W. C., and Southard, J. B. (2005). Experiments on oscillatory-flow and combined-flow bed forms: implications for interpreting parts of the shallow-marine sedimentary record. *J. Sediment. Res.* 75, 501–513. doi: 10.2110/jsr.2005.039
- Dunham, R. J. (1962). "Classification of carbonate rocks according to depositional texture," in *Classification of Carbonate Rocks—a Symposium*, ed. W. E. Ham (Tulsa, OK: American Association of Petroleum Geologists), 108–121.
- Embry, A., and Klován, J. E. (1971). A late devonian reef tract on northeastern Banks Island, NWT. *Bull. Can. Pet. Geol.* 19, 730.
- Franzese, J., Spalletti, L., Pérez, I. G., and Macdonald, D. (2003). Tectonic and paleoenvironmental evolution of Mesozoic sedimentary basins along the Andean foothills of Argentina (32°–54°S). *J. South Am. Earth Sci.* 16, 81–90. doi: 10.1016/S0895-9811(03)00020-8
- Galland, O., Hallot, E., Cobbold, P. R., Ruffet, G., and de Bremond d'Ars, J. (2007). Volcanism in a compressional andean setting: a structural and geochronological study of Tromen volcano (Neuquén province, Argentina). *Tectonics* 26:TC4010. doi: 10.1029/2006TC002011
- Galloway, W. E. (1975). "Process framework for describing the morphologic and stratigraphic evolution of deltaic depositional systems," in *Deltas: Models for Exploration*, ed. M. L. Broussard (Houston: Houston Geological Society), 87–98.
- Gugliotta, M., Flint, S. S., Hodgson, D. M., and Veiga, G. D. (2016). Recognition criteria, characteristics and implications of the fluvial to marine transition zone in ancient deltaic deposits (Lajas Formation, Argentina). *Sedimentology* 63, 1971–2001. doi: 10.1111/sed.12291
- Harms, J. C., Southard, J. B., Spearing, D. R., and Walker, R. G. (1975). "Stratification and sequence in prograding shoreline deposits," in *Depositional Environments as Interpreted From Primary Sedimentary Structures and Stratification Sequences*, eds J. C. Harms, J. B. Southard, D. R. Spearing, and R. G. Walker (Tulsa, OK: SEPM Short course), 81–102. doi: 10.2110/scn.75.01.0081
- Holland-Hansen, W., and Martinsen, O. J. (1996). Shoreline trajectories and sequences; description of variable depositional-dip scenarios. *J. Sediment. Res.* 66, 670–688. doi: 10.1306/d42683dd-2b26-11d7-8648000102c1865d
- Holbrook, J. M., and Miall, A. D. (2020). Time in the rock: a field guide to interpreting past events and processes from siliciclastic stratigraphy. *EarthSci. Rev.* 203:103121. doi: 10.1016/j.earscirev.2020.103121
- Howell, J. A., Schwarz, E., Spalletti, L. A., and Veiga, G. D. (2005). The Neuquén Basin: an overview. *Geol. Soc. Lon. Spec. Publ.* 252, 1–14. doi: 10.1144/gsl.sp.2005.252.01.01
- Jordan, O. D., Gupta, S., Hampson, G. J., and Johnson, H. D. (2016). Preserved stratigraphic architecture and evolution of a net-transgressive mixed wave- and tide-influenced coastal system: the cliff house sandstone, Northwestern New Mexico, U.S.A. *J. Sediment. Res.* 86, 1399–1424. doi: 10.2110/jsr.2016.83
- Klein, G. D. (1970). Depositional and dispersal dynamics of intertidal sand bars. *J. Sediment. Res.* 40, 1095–1127. doi: 10.1306/74d72144-2b21-11d7-8648000102c1865d
- Lanier, W. P., Tessier, B., Alexander, C. R., Davis, R. A., and Henry, V. J. (1998). Climbing-ripple bedding in the fluvio-estuarine transition; a common feature associated with tidal dynamics (modern and ancient analogues). *Spec. Publ. Soc. Sediment. Geol.* 61, 109–117. doi: 10.2110/pec.98.61.0109
- Lazo, D. G. (2007). Análisis tafonómico e inferencia del grado de mezcla temporal y espacial de la macrofauna del Miembro Pilmatué de la Formación Agrio, Cretácico Inferior de cuenca Neuquina, Argentina. *Ameghiniana* 43, 311–326.
- Leckie, D. A., and Walker, R. G. (1982). Storm- and tide-dominated shorelines in cretaceous moosebar-lower gates interval—outcrop equivalents of deep basin gas trap in western Canada. *AAPG Bull.* 66, 138–157.
- Legarreta, L., and Gulisano, C. A. (1989). "Análisis estratigráfico secuencial de la Cuenca Neuquina (Triásico superior-Terciario inferior, Argentina)," in *Cuencas Sedimentarias Argentinas*, eds G. Chebli and L. Spalletti (San Miguel de Tucumán: Universidad Nacional de Tucumán), 221–243.
- Legarreta, L., and Uliana, M. A. (1991). "Jurassic—marine oscillations and geometry of back-arc basin fill, central argentine andes," in *Sedimentation, Tectonics and Eustasy Sea level Changes at Active Plate Margins*, ed. D. I. M. MacDonald (Oxford: International Association of Sedimentologists Special Publication), 429–450. doi: 10.1002/9781444303896.ch23
- Legler, B., Hampson, G. J., Jackson, C. A. L., Johnson, H. D., Massart, B. Y. G., and Sarginson, M. (2014). Facies relationships and stratigraphic architecture of distal, mixed tide- and wave-influenced deltaic deposits: lower Sego Sandstone, Western Colorado, U.S.A. *J. Sediment. Res.* 84, 605–625. doi: 10.2110/jsr.2014.49
- Leva López, J., Rossi, V. M., Olariu, C., and Steel, R. J. (2016). Architecture and recognition criteria of ancient shelf ridges; an example from campanian almond formation in hanna basin. *USA. Sedimentol.* 63, 1651–1676. doi: 10.1111/sed.12279
- Miall, A. D. (2015). Updating uniformitarianism: stratigraphy as just a set of 'frozen accidents'. *Geol. Soc. Lon. Spec. Publ.* 404, 11–36. doi: 10.1144/sp404.4
- Nichols, G. (2009). *Sedimentology and Stratigraphy*. Chichester: Wiley-Blackwell.
- Olariu, C. (2014). "Autogenic process change in modern deltas," in *From Depositional Systems to Sedimentary Successions on the Norwegian Continental Margin*, Vol. 46, eds A. W. Martinius, R. Ravnås, J. A. Howell, R. J. Steel, and J. P. Wonham (Oxford: International Association of Sedimentologists Special Publication), 149–166. doi: 10.1002/9781118920435.ch7
- Olariu, C., Steel, R. J., Dalrymple, R. W., and Gingras, M. K. (2012). Tidal dunes versus tidal bars: the sedimentological and architectural characteristics of compound dunes in a tidal seaway, the lower baronia sandstone (Lower Eocene), Ager Basin, Spain. *Sediment. Geol.* 279, 134–155. doi: 10.1016/j.sedgeo.2012.07.018
- Olsen, T. R., Mellere, D., and Olsen, T. (1999). Facies architecture and geometry of landward-stepping shoreface tongues: the Upper Cretaceous Cliff House Sandstone (Mancos Canyon, south-west Colorado). *Sedimentology* 46, 603–625. doi: 10.1046/j.1365-3091.1999.00234.x
- Painter, C. S., York-Sowecke, C. C., and Carrapa, B. (2013). Sequence stratigraphy of the Upper Cretaceous Sego Sandstone Member reveals spatio-temporal changes in depositional processes, Northwest Colorado, U.S.A. *J. Sediment. Res.* 83, 323–338. doi: 10.2110/jsr.2013.21
- Peng, Y., Steel, R. J., Rossi, V. M., and Olariu, C. (2018). Mixed-energy process interactions read from a compound-clinoform delta (paleo-Orioco Delta, Trinidad): preservation of river and tide signals by mud-induced wave damping. *J. Sediment. Res.* 88, 75–90. doi: 10.2110/jsr.2018.3
- Reeder, S. L., and Rankey, E. C. (2008). Interactions between tidal flows and ooid shoals, northern Bahamas. *J. Sediment. Res.* 78, 175–186. doi: 10.2110/jsr.2008.020
- Reineck, H.-E. (1963). *Sedimentgefüge im Bereich der Südlichen Nordsee*. Frankfurt: Waldemar Kramer.
- Rodriguez, A. B., Simms, A. R., and Anderson, J. B. (2010). Bay-head deltas across the northern gulf of Mexico back step in response to the 8.2 ka cooling event. *Q. Sci. Rev.* 29, 3983–3993. doi: 10.1016/j.quascirev.2010.10.004
- Rossi, V. M., Perillo, M. M., Steel, R. J., and Olariu, C. (2017). Quantifying mixed-process variability in shallow-marine depositional systems: what are

- sedimentary structures really telling us? *J. Sediment. Res.* 87, 1060–1074. doi: 10.2110/jsr.2017.49
- Rossi, V. M., and Steel, R. J. (2016). The role of tidal, wave and river currents in the evolution of mixed-energy deltas: example from the Lajas Formation (Argentina). *Sedimentology* 63, 824–864. doi: 10.1111/sed.12240
- Sadler, P. M. (1981). Sediment accumulation rates and the completeness of stratigraphic sections. *J. Geol.* 89, 569–584. doi: 10.1086/628623
- Schwarz, E. (1999). *Facies sedimentarias y Modelo Depositional de la Formación Mulichinco (Valanginiano), Cuenca Neuquina Septentrional. Revista de la Asociación Argentina de Sedimentología [Online]*, Vol. 6. Available: http://www.scielo.org.ar/scielo.php?script=sci_arttext&pid=S1853-63601999000100003&lng=es&tlng=es (accessed October 18, 2018).
- Schwarz, E. (2012). Sharp-based marine sandstone bodies in the mulichinco formation (Lower Cretaceous), neuquén basin, argentina: remnants of transgressive offshore sand ridges. *Sedimentology* 59, 1478–1508. doi: 10.1111/j.1365-3091.2011.01314.x
- Schwarz, E., Álvarez-Trentini, G., and Valenzuela, M. E. (2013). Ciclos mixtos carbonáticos/silicoclásticos en el Miembro superior de la Formación Mulichinco (Yacimiento Cañadón Amarillo, Cuenca Neuquina central, Argentina): implicancias secuenciales y para caracterización de reservorios. *Latin Am. J. Sedimentol. Basin Anal.* 20, 21–49.
- Schwarz, E., and Howell, J. A. (2005). Sedimentary evolution and depositional architecture of a lowstand sequence set: the lower cretaceous mulichinco formation. Neuquén Basin, Argentina. *Geol. Soc. Lond. Spec. Publ.* 252, 109–138. doi: 10.1144/gsl.sp.2005.252.01.06
- Schwarz, E., Spalletti, L. A., and Howell, J. A. (2006). Sedimentary response to a tectonically induced sea-level fall in a shallow back-arc basin: the mulichinco formation (Lower Cretaceous), Neuquén Basin, Argentina. *Sedimentology* 53, 55–81. doi: 10.1111/j.1365-3091.2005.00753.x
- Schwarz, E., Veiga, G. D., Álvarez-Trentini, G., Isla, M. F., and Spalletti, L. A. (2018). Expanding the spectrum of shallow-marine, mixed carbonate-siliciclastic systems: processes, facies distribution and depositional controls of a siliciclastic-dominated example. *Sedimentology* 65, 1558–1589. doi: 10.1111/sed.12438
- Schwarz, E., Veiga, G. D., Álvarez-Trentini, G., and Spalletti, L. A. (2016). Climatically versus eustatically controlled, sediment-supply-driven cycles: carbonate-siliciclastic, high-frequency sequences in the Valanginian of the Neuquén Basin (Argentina). *J. Sediment. Res.* 86, 312–335. doi: 10.2110/jsr.2016.21
- Simms, A. R., Anderson, J. B., and Blum, M. (2006). Barrier-island aggradation via inlet migration: mustang Island, Texas. *Sediment. Geol.* 187, 105–125. doi: 10.1016/j.sedgeo.2005.12.023
- Sisulak, C. F., and Dashtgard, S. E. (2012). Seasonal controls on the development and character of inclined heterolithic stratification in a tide-influenced, fluvially dominated channel: fraser River, Canada. *J. Sediment. Res.* 82, 244–257. doi: 10.2110/jsr.2012.21
- Sixsmith, P. J., Hampson, G. J., Gupta, S., Johnson, H. D., and Fofana, J. F. (2008). Facies architecture of a net transgressive sandstone reservoir analog: the cretaceous hosta tongue. New Mexico. *AAPG Bull.* 92, 513–547. doi: 10.1306/01020807017
- Spalletti, L. A., Franzese, J. R., Matheos, S. D., and Schwarz, E. (2000). Sequence stratigraphy of a tidally dominated carbonate-siliciclastic ramp; the Tithonian-Early Berriasian of the Southern Neuquén Basin, Argentina. *J. Geol. Soc.* 157, 433–446. doi: 10.1144/jgs.157.2.433
- Swift, D. J. P., and Thorne, J. A. (1991). “Sedimentation on continental margins, I: a general model for shelf sedimentation,” in *Shelf Sand and Sandstone Bodies: Geometry, Facies and Sequence Stratigraphy*, eds D. J. P. Swift, G. F. Oertel, R. W. Tillman, and J. A. Thorne (Oxford: Blackwell Scientific Publications), 3–31.
- Taylor, A. M., and Goldring, R. (1993). Description and analysis of bioturbation and ichnofabric. *J. Geol. Soc.* 150, 141–148. doi: 10.1144/gsjgs.150.1.0141
- Thomas, R. G., Smith, D. G., Wood, J. M., Visser, J., Calverley-Range, E. A., and Koster, E. H. (1987). Inclined heterolithic stratification—Terminology, description, interpretation and significance. *Sediment. Geol.* 53, 123–179. doi: 10.1016/S0037-0738(87)80006-4
- Vakarelov, B. K., and Ainsworth, R. B. (2013). A hierarchical approach to architectural classification in marginal-marine systems: Bridging the gap between sedimentology and sequence stratigraphy. *AAPG Bull.* 97, 1121–1161. doi: 10.1306/11011212024
- Vakarelov, B. K., Ainsworth, R. B., and MacEachern, J. A. (2012). Recognition of wave-dominated, tide-influenced shoreline systems in the rock record: variations from a microtidal shoreline model. *Sediment. Geol.* 279, 23–41. doi: 10.1016/j.sedgeo.2011.03.004
- Van Cappelle, M., Ravnås, R., Hampson, G. J., and Johnson, H. D. (2017). Depositional evolution of a progradational to aggradational, mixed-influenced deltaic succession: jurassic Tofte and Ile formations, southern Halten Terrace, offshore Norway. *Mar. Pet. Geol.* 80, 1–22. doi: 10.1016/j.marpetgeo.2016.11.013
- Van Cappelle, M., Stukins, S., Hampson, G. J., and Johnson, H. D. (2016). Fluvial to tidal transition in proximal, mixed tide-influenced and wave-influenced deltaic deposits: cretaceous lower Sego Sandstone. Utah, USA. *Sedimentology* 63, 1333–1361. doi: 10.1111/sed.12267
- Vaucher, R., Pittet, B., Hormière, H., Martin, E. L. O., and Lefebvre, B. (2017). A wave-dominated, tide-modulated model for the lower ordovician of the anti-atlas. Morocco. *Sedimentology* 64, 777–807. doi: 10.1111/sed.12327
- Vergani, G. D., Tankard, A. J., Belotti, H. J., and Welsink, H. J. (1995). “Tectonic evolution and paleogeography of the Neuquén Basin, Argentina,” in *Petroleum Basins of South America*, eds A. J. Tankard, R. Suárez Soruco, and H. J. Welsink (Tulsa, OK: AAPG Memoir), 383–402.
- Wei, X. J., Steel, R. J., Ravnas, R., Jiang, Z. X., Olariu, C., and Li, Z. Y. (2016). Variability of tidal signals in the Brent Delta Front: new observations on the Rannoch Formation, northern North Sea. *Sediment. Geol.* 335, 166–179. doi: 10.1016/j.sedgeo.2016.02.012
- Wesolowski, L. J. N., Buatois, L. A., Mángano, M. G., Ponce, J. J., and Carmona, N. B. (2018). Trace fossils, sedimentary facies and parasequence architecture from the lower cretaceous mulichinco formation of argentina: the role of fair-weather waves in shoreface deposits. *Sediment. Geol.* 367, 146–163. doi: 10.1016/j.sedgeo.2018.02.007
- Westoby, M. J., Brasington, J., Glasser, N. F., Hambrey, M. J., and Reynolds, J. M. (2012). ‘Structure-from-Motion’ photogrammetry: a low-cost, effective tool for geoscience applications. *Geomorphology* 179, 300–314. doi: 10.1016/j.geomorph.2012.08.021
- Willis, B. J., and Gabel, S. (2001). Sharp-based, tide-dominated deltas of the Sego Sandstone, Book Cliffs, Utah, USA. *Sedimentology* 48, 479–506. doi: 10.1046/j.1365-3091.2001.00363.x
- Willis, B. J., and Gabel, S. (2003). Formation of deep incisions into tide-dominated river deltas: implications for the stratigraphy of the Sego Sandstone. Book Cliffs, Utah, U.S.A. *J. Sediment. Res.* 73, 246–263. doi: 10.1306/090602730246
- Wright, V. P. (1992). A revised classification of limestones. *Sediment. Geol.* 76, 177–185. doi: 10.1016/0037-0738(92)90082-3
- Yang, B. C., Dalrymple, R. W., and Chun, S. S. (2005). Sedimentation on a wave-dominated, open-coast tidal flat, south-western Korea: summer tidal flat – winter shoreface. *Sedimentology* 52, 235–252. doi: 10.1111/j.1365-3091.2004.00692.x
- Yokokawa, M., Kishi, M., Masuda, F., and Yamanaka, M. (1995). “Climbing ripples recording the change of tidal current condition in the middle Pleistocene Shimosa Group, Japan,” in *Tidal Signatures in Modern and Ancient Sediments*, eds B. W. Flemming and A. Bartholomä (Blackwell Science Ltd), 301–312.
- Yoshida, S., Steel, R. J., and Dalrymple, R. W. (2007). Changes in depositional processes - An ingredient in a new generation of sequence-stratigraphic models. *J. Sediment. Res.* 77, 447–460. doi: 10.2110/jsr.2007.048

Conflict of Interest: The authors declare that the research was conducted in the absence of any commercial or financial relationships that could be construed as a potential conflict of interest.

Copyright © 2020 Sleveland, Midtkandal, Galland and Leanza. This is an open-access article distributed under the terms of the Creative Commons Attribution License (CC BY). The use, distribution or reproduction in other forums is permitted, provided the original author(s) and the copyright owner(s) are credited and that the original publication in this journal is cited, in accordance with accepted academic practice. No use, distribution or reproduction is permitted which does not comply with these terms.